

## Repulsion-driven metallic phase in the ground state of the half-filled $t$ - $t'$ ionic Hubbard chain

Gerardo L. Rossini<sup>1</sup> and George I. Japaridze<sup>2,3</sup>

<sup>1</sup>*IFLYSIB-CONICET and Departamento de Física, Universidad Nacional de La Plata, 1900 La Plata, Argentina*

<sup>2</sup>*Center of Condensed Matter Physics and Quantum Computations, Ilia State University, Cholokashvili Avenue 3-5, 0162 Tbilisi, Georgia*

<sup>3</sup>*Andronikashvili Institute of Physics, Tamarashvili str. 6, 0177 Tbilisi, Georgia*



(Received 17 April 2023; revised 26 October 2023; accepted 14 November 2023; published 6 December 2023)

An unusual metallic phase is argued to develop in the one-dimensional ionic Hubbard model, at half-filling and zero magnetization, at intermediate electron-electron repulsion  $U$  when second-neighbors hopping is allowed and tuned close to a topological Lifshitz transition (connected with a change of the Fermi surface in the noninteracting system). The metallic state lies between a band insulator phase at low repulsion and a correlated (Mott-like) insulator phase at high repulsion. In approaching the latter, the model supports short-range antiferromagnetic order and spontaneous dimerization of both bond charge and nearest-neighbor antiferromagnetic correlations. A combination of mean-field and effective-field theory (bosonization) provides an analytical understanding of the physical processes underlying the argued phase transitions. The ground and low-energy excited states of finite-length chains are explored by density-matrix renormalization-group (DMRG) calculations, providing numerical evidence for the intermediate gapless phase. Such finite systems are attainable by cold atoms in optical lattices for a wide range of the parameter  $U$ .

DOI: [10.1103/PhysRevA.108.063307](https://doi.org/10.1103/PhysRevA.108.063307)

### I. INTRODUCTION

Atomic gases stored in artificially engineered optical lattices offer an unique possibility to simulate and study condensed-matter systems with unconventional, or less achievable in actual materials, properties [1–3]. Among the advantages of these systems is the possibility to manipulate the strength of the interaction using the Feshbach resonance [4], which enables monitoring of the evolution of the ground-state properties of the quantum many-body system with interaction, starting from the weak coupling till the limit of very strong interaction. Competition between the (kinetic) delocalization energy and interaction is profoundly seen in low-dimensional quantum systems and leads to a very rich set of many-body phases displayed in the remarkable ground-state (GS) properties of these systems [5,6].

Optical lattices can be generated in various geometries, including two-dimensional triangular [7,8], kagome [9], and hexagonal [10,11] structures as well as quasi-one-dimensional few-chain systems with zigzag [12] or ladder [13,14] geometry. In addition, the optical engineering allows the details of the lattice structure to be manipulated, in particular to introduce a bias for atom occupation energy on neighboring sites and thus to create a bipartite lattice [15,16] or ladder with nonequivalent legs [17]. This makes the ground-state phase diagram of the system even more complex and opens the possibility to experimentally investigate the nature of various quantum phase transitions between different phases with remarkable properties. In particular, fermionic atomic gases with repulsion on optical lattices provide an excellent testing ground to study *insulator-insulator* and *metal-insulator* transitions driven by the interplay between the effects caused by correlations, geometrical frustration, and nonequivalence of atomic sublattices [18–20]. Also, emergent effects connected

with the topological Lifshitz transition [21] are of prime current interest [22–27].

In this paper we consider the one-dimensional model of interacting fermions given by the following Hamiltonian:

$$\begin{aligned} \mathcal{H} = & -t \sum_{i,\sigma}^L (c_{i,\sigma}^\dagger c_{i+1,\sigma} + \text{H.c.}) \\ & + t' \sum_{i,\sigma}^L (c_{i,\sigma}^\dagger c_{i+2,\sigma} + \text{H.c.}) \\ & + \frac{\Delta}{2} \sum_{i,\sigma}^L (-1)^i n_{i,\sigma} + U \sum_i n_{i,\uparrow} n_{i,\downarrow}. \end{aligned} \quad (1)$$

Here,  $c_{i,\sigma}^\dagger$  ( $c_{i,\sigma}$ ) creates (annihilates) a fermion with spin  $\sigma = \uparrow, \downarrow$  on site  $i$  and  $n_{i,\sigma} = c_{i,\sigma}^\dagger c_{i,\sigma}$  is the spin  $\sigma$  particle density operator. The nearest-neighbor (n.n.) hopping amplitude is denoted by  $t$ , the next-to-nearest-neighbor (n.n.n.) hopping amplitude by  $t'$  ( $t, t' > 0$ ),  $\Delta$  is the potential energy difference between neighboring sites, and  $U$  is the on-site Coulomb repulsion. The Hamiltonian (1) commutes with the number operator of particles with spin  $\sigma$ ,  $\mathcal{N}_\sigma = \sum_i n_{i,\sigma}$ . Below in this paper we restrict our consideration to the case of the half-filled band with zero magnetization, with particle number eigenvalues  $N_\uparrow = N_\downarrow = L/2$ , and to repulsive interaction  $U > 0$ .

For  $\Delta = 0$ , the Hamiltonian corresponds to the  $t$ - $t'$  Hubbard model [28,29] in the case of the half-filled band, the prototype model to study the metal-insulator transition in one dimension [30–35]. At  $t' < 0.5t$  the system is in a gapped insulating phase for arbitrary  $U > 0$ , but at  $t' > 0.5t$  is characterized by the quantum phase transition from a charge gapless metallic behavior at  $U < U_c$  into an insulating phase at  $U > U_c$  [30–32]. The qualitative change of the ground-state

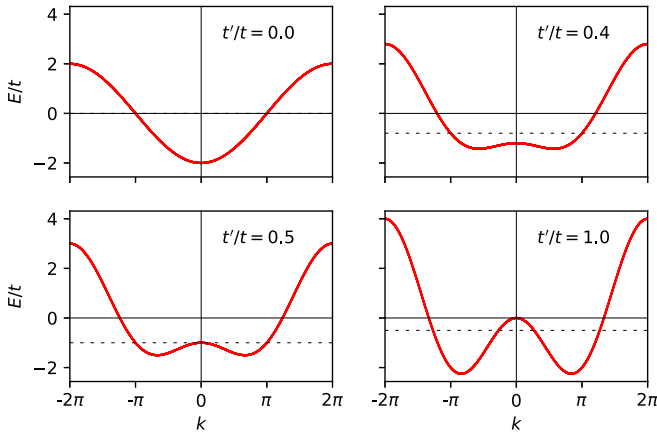


FIG. 1. Dispersion relation  $E_k$  for the  $t$ - $t'$  (nonionic,  $\Delta = 0$ ) chain at different values of  $t'/t$ . The dashed line indicates the chemical potential at half-filling. At  $t' = 0.5t$  a Lifshitz transition takes place, changing the structure of the Fermi surface from two to four Fermi points.

properties of the system at  $t' > 0.5t$  emerges as the result of the topological Lifshitz transition in the ground state of the free system, where the number of Fermi points doubles [29] (see Fig. 1). It has been shown that at fixed  $U$  and increasing  $t'$  the insulator-to-metal transition is described in terms of the commensurate-incommensurate transition [36,37] with a transition curve determined by the relation  $M_c(U) = 2t'_c - t'^2/t'_c$ , where  $M_c(U)$  is the charge (Hubbard) gap at the given  $U$  and  $t' = 0$  [34].

For  $t' = 0$  and  $\Delta \neq 0$  the Hamiltonian (1) describes the ionic Hubbard model (IHM) [38–41]. At finite  $\Delta$  the translational invariance is explicitly broken, the lattice unit is doubled, and the density imbalance between neighboring sites shows up via the presence of a long-range-ordered (LRO) charge density wave (CDW) pattern in the ground state for arbitrary  $U > 0$  [43]. On the other hand, the repulsive Hubbard interaction suppresses density inhomogeneities and favors antiferromagnetic ordering on neighboring sites. Competition between these tendencies is resolved in the ground-state phase diagram via the presence of two, excluding each other, phase sectors—the band insulating CDW phase at  $U < U_{c1}$  and correlated Mott insulating phases at  $U > U_{c2}$ , separated by a narrow intermediate bond-ordered wave (BOW) phase [41]. The nature of the corresponding phase transitions has been also first established within the continuum-limit bosonization description, showing the Ising type (charge) transition at  $U_{c1}$  from a CDW band insulator phase to a BOW insulator phase and the second (spin) Kosterlitz-Thouless type transition at  $U_{c2}$  from the BOW to a correlated Mott insulator [41]. Subsequent numerical studies have unambiguously proven this phase diagram [42–46].

At  $U = 0$  the model can be easily diagonalized in the momentum space (see Appendix A). For  $t' < t'_* = 0.5t\sqrt{1 + (\Delta/2t)^2} - \Delta/8$  (assuming  $\Delta > 0$ ) the ground state corresponds to the standard CDW band insulator with direct gap, at  $t'_* < t' < t'_c$  to the band insulator (BI) with indirect gap and at  $t' > t'_c = 0.5t\sqrt{1 + (\Delta/2t)^2} + \Delta/8$  to the metal. In this case the Lifshitz transition is shaded

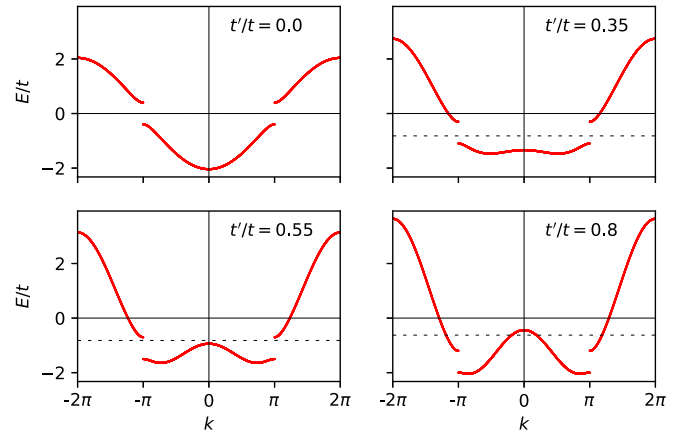


FIG. 2. Dispersion relation  $E_k$  for the  $t$ - $t'$  ionic chain at  $\Delta = 0.8t$  and different values of  $t'/t$ . The dashed line indicates the chemical potential at half-filling. The panels with  $t' = 0.0, 0.35t$  show a band insulator with direct gap, while the one with  $t' = 0.55t$  illustrates an indirect gap and quadratic dispersion for quasiparticles and holes close to the insulator-metal transition. In the panel with  $t' = 0.8t$  the system becomes gapless, with well-defined linear dispersion for quasiparticles and holes around four Fermi points. The unit cell has two sites; here the Brillouin zone is expanded to show the two dispersion branches side by side.

by the presence of the band gap and displays itself in the insulator-metal transition, where a Fermi surface with four points opens (see Fig. 2).

Inclusion of the Hubbard repulsion into the scheme introduces an additional set of complexity: both the metal and insulating phases experience transition into different insulating phases at strong repulsion. In a recent publication this problem has been addressed within the mean-field approximation [47]. It has been shown that unconventional insulating phases, characterized by a spin and charge-density modulation with a wavelength equal to four lattice units, become energetically favorable above the Lifshitz transition and almost completely wipe out the metallic phases. This type of density modulations are absolutely natural for the interacting fermions with n.n.n. hopping and emerge in the system at  $t' \gg t'_c$  as a result of the opening of four Fermi points and the explicit breaking of translational symmetry by the finite ionic term.

However, in the direct proximity of the insulator-metal (Lifshitz) transition, at  $t'_* < t' < t'_c$ , metallic properties of the free system are described by particles and holes with quadratic dispersion, and thus details of the phase diagram deserve a more accurate analysis than the previous mean-field approximation. In this paper we address this problem and find a different scenario. An analytical study based on both an improved mean-field approximation and tailored bosonization tools allows the underlying physical processes responsible for the complex nature of the phase diagram to be understood.

Density-matrix renormalization group (DMRG) computations, setting  $t, t'$ , and  $\Delta$  where the noninteracting system is gapped but close to the Lifshitz point, support the existence of a metallic phase at intermediate Hubbard repulsion  $U$ . Though at present we are not able to properly extrapolate finite size results into a controlled thermodynamic limit, our numerical

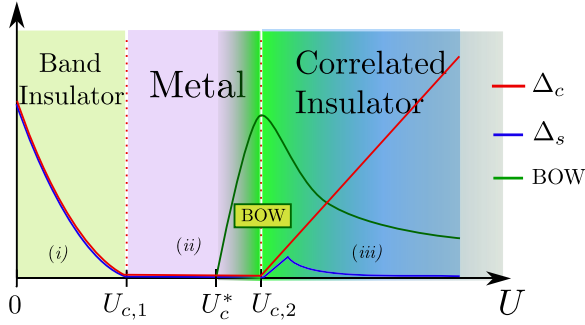


FIG. 3. Schematic phase diagram suggested by our numerical results. Fixed  $t'/t$  is tuned so that the noninteracting system is close to the Lifshitz transition, still bearing an indirect excitation gap (see Fig. 2, lower left panel). The Hubbard repulsion  $U$  drives the system from a band insulator into an unconventional metal ( $U_{c,1}$ ) before reaching the correlated insulator phase ( $U_{c,2}$ ). The charge gap  $\Delta_c$  is plotted in red, the spin gap  $\Delta_s$  in blue, and the BOW order amplitude in green. Areas in solid colors identify the ground-state phase according to the charge gap, while the green gradient indicates the presence of spontaneous BOW order ( $U > U_c^*$ ) starting inside the metallic phase.

exploration suggests the picture shown in Fig. 3. In the considered range of parameters, the ground-state phase diagram of the system as a function of the on-site Hubbard repulsion  $U$  consists of three phases: at  $0 < U < U_{c,1}$  the band insulating CDW phase, for  $U_{c,1} < U < U_{c,2}$  a repulsion driven metallic phase, and for  $U > U_{c,2}$  a correlated insulator (CI) phase. The LRO CDW pattern is clearly present, with decreasing amplitude, in all these phases. A spontaneous BOW order appears inside the metallic phase, with increasing amplitude towards its edge; this amplitude starts to decay as soon as the charge gap reopens, however it remains finite in the CI phase and continuously evolves into the spin dimerization pattern at  $U \rightarrow \infty$ .

The paper is organized as follows. In Sec. II A we present a mean-field approach leading to a renormalization of the ionicity parameter  $\Delta$  due to electron-electron interactions; we explore the appearance of a metallic phase within this regime. In Sec. II B we introduce a bosonization scheme allowing the role of ionicity  $\Delta$ , Hubbard repulsion  $U$  and n.n.n. hopping  $t'$  to be analyzed on equal footing; within this framework we discuss the different possible ground-state phases of the present model. We also identify a parameter region where such phases are realized. In Sec. III we numerically explore the model with the DMRG technique, selecting intermediate  $t'$  and  $\Delta$  and a full range for the Hubbard repulsion  $U$ . Finally, in Sec. IV we summarize and discuss the obtained results.

## II. QUALITATIVE ESTIMATIONS

### A. Self-consistent approach

Because the translation symmetry of the system is explicitly broken by the  $\Delta$  term in Eq. (1), an alternating pattern of charge density is present in the ground state at arbitrary  $U$  [43]. For further analysis it is convenient to subtract from the density operators their vacuum expectation values, rewriting

them in the following way:

$$n_{i,\sigma} = \frac{1}{2}[1 - (-1)^i \delta \rho_0(U)] + :n_{i,\sigma} :, \quad (2)$$

where  $::$  denote fluctuations on top of the GS value and  $\delta \rho_0(U)$  is the amplitude of the CDW pattern present in the ground state at given  $U$ . Here, we take into account that  $\langle n_{i,\uparrow} \rangle = \langle n_{i,\downarrow} \rangle$ . Using Eq. (2), the Hamiltonian in Eq. (1) can be rewritten in the following way:

$$\begin{aligned} \mathcal{H} = & -t \sum_{i,\sigma} (c_{i,\sigma}^\dagger c_{i+1,\sigma} + \text{H.c.}) \\ & + t' \sum_{i,\sigma} (c_{i,\sigma}^\dagger c_{i+2,\sigma} + \text{H.c.}) \\ & + \frac{\Delta_r}{2} \sum_{i,\sigma} (-1)^i :n_{i,\sigma} : + U \sum_i :n_{i,\uparrow} :: n_{i,\downarrow} :, \quad (3) \end{aligned}$$

where

$$\Delta_r(U) = \Delta - U \delta \rho_0(U). \quad (4)$$

Thus, even in the gapped band insulating phase, where the charge fluctuations are suppressed and at weak coupling one could ignore their interaction in the last term of Eq. (3), the contribution of the on-site Hubbard term is crucial and manifest in the renormalization of the ionic gap given in Eq. (4).

Below in this subsection we restrict our consideration to the mean-field approximation and neglect the scattering of quasiparticles (blocked by the band gap) on top of the Fermi surface given by the last term in Eq. (3). In this case the Hamiltonian can be easily diagonalized in momentum space (see Appendix A) to give

$$\mathcal{H}_{t-t'-\Delta_r} = \sum_{k,\sigma} (E_k^- \alpha_{k,\sigma}^\dagger \alpha_{k,\sigma} + E_k^+ \beta_{k,\sigma}^\dagger \beta_{k,\sigma}), \quad (5)$$

where

$$E_k^\pm = \varepsilon'_k \pm \sqrt{\varepsilon_k^2 + (\Delta_r/2)^2} \quad (6)$$

are the energy dispersions for  $\alpha$  and  $\beta$  quasiparticles, corresponding to the “lower” and “upper” bands, respectively.

In the ground state of the half-filled system the  $L$  lowest energy states are filled and the rest  $L$  are empty. For  $t' \leq 0.5t$ ,  $E_k^-$  and  $E_k^+$  are separated with a direct gap equal to  $\Delta_r$ ; all states in the lower band are occupied, whereas in the upper band all states are empty; the system is in the insulating state. For  $t' > 0.5t$ , with increasing  $t'$  (or reducing  $\Delta_r$ ) bands might overlap, due to the  $k$ -dependent energy shift  $\varepsilon'_k$ , and the system experience a transition into the metallic phase.

At given values of the parameters  $t$  and  $t'$ , it is useful to introduce a critical value of the effective ionicity parameter  $\Delta_r^{\text{cr}} \geq 0$ ,

$$\Delta_r^{\text{cr}} = \begin{cases} 4t' - t^2/t' & \text{for } t' \geq 0.5t, \\ 0 & \text{otherwise,} \end{cases} \quad (7)$$

corresponding to the metal-insulator transition: for  $|\Delta_r| > \Delta_r^{\text{cr}}$  ( $|\Delta_r| < \Delta_r^{\text{cr}}$ ), the system is in an insulating (metallic) state. Note that for  $t' < 0.5t$  the system remains in the insulating phase for any finite value of  $|\Delta_r|$ .

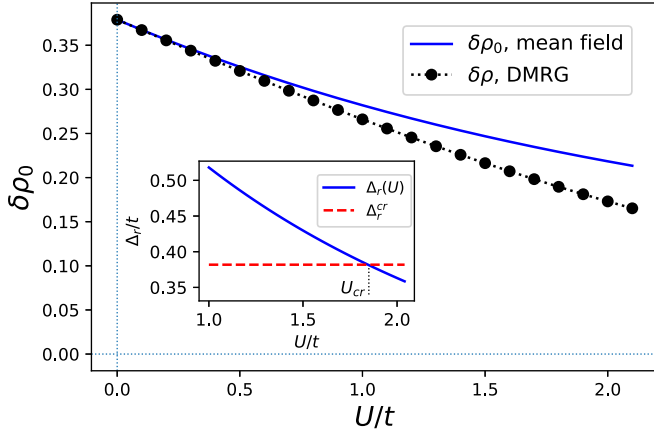


FIG. 4. The self-consistent solution for  $\delta\rho_0(U)$  computed for  $t' = 0.55t$ ,  $\Delta = 0.8t$  is shown in solid blue. Actual DMRG data for  $\delta\rho(U)$  is shown in black dots for comparison. Inset: self-consistent solution for the renormalized  $\Delta_r$  as a function of  $U$  (in solid blue). The dashed red line is the critical value for gap closing,  $\Delta_r^{\text{cr}} = 4t' - t^2/t'$ . The intersection occurs at  $U_{\text{cr}} \approx 1.85t$ .

Inserting in Eq. (4) the analytical expression for the amplitude of the CDW modulation in the insulating phase,

$$\delta\rho_0 = \frac{\Delta_r \kappa K(\kappa)}{2\pi t}, \quad (8)$$

where  $K(\kappa)$  is the complete elliptic integral of the first kind with the modulus  $\kappa(t, \Delta_r) = [1 + (\Delta_r/4t)^2]^{-1/2}$  [see Eq. (A20) in Appendix A], we obtain a self-consistent equation for  $\Delta_r$ ,

$$\Delta_r = \Delta - \frac{U \Delta_r \kappa(t, \Delta_r) K[\kappa(t, \Delta_r)]}{2\pi t}, \quad (9)$$

that can be solved iteratively for given  $U$ .

The results, for  $t' = 0.55t$  and  $\Delta = 0.8t$ , are shown in Fig. 4. In the inset we first show the renormalized  $\Delta_r$  as a function of  $U$ : one can see that  $U$  competes with the bare ionicity  $\Delta$ , reducing  $\Delta_r$ . Eventually, provided  $t' > 0.5t$ , the band gap closes at a critical point  $U_{\text{cr}}$  when

$$\Delta_r(U_{\text{cr}}) = \Delta_r^{\text{cr}} \equiv 4t' - t^2/t', \quad (10)$$

driving the system into a metallic phase. For the given parameters this occurs at  $U_{\text{cr}} \approx 1.85t$ , in qualitative agreement with  $U_{c,1} \approx 2.2t$  suggested by the DMRG data discussed in Sec. III A.

Once having  $\Delta_r(U)$ , one can compute the CDW amplitude  $\delta\rho_0(U)$  from Eq. (8), which is shown in the main panel of Fig. 4, in good agreement with exact DMRG data discussed in Sec. III B 1. Notice that as the renormalized  $\Delta_r$  decreases, the CDW amplitude is also reduced by electron repulsion  $U$ .

### B. Bosonization approach

In this subsection we use the bosonization technique to obtain a qualitative description of the low-energy properties of the Hamiltonian in Eq. (3). We restrict our consideration to the weak-coupling case  $\Delta_r, U \ll t$  and  $t' \simeq 0.5t$ , i.e., the close proximity to the insulator-metal transition.

Because for the selected set of model parameters the spectrum of the free system is either gapped or, in a metallic phase, has a quadratic dispersion, the straightforward application of the bosonization technique is not possible. Therefore, we follow the route developed earlier in studies of the standard IHM [41], where one starts the description from the weak-coupling case, linearizes the spectrum in the vicinity of the two Fermi points  $k_F = \pm\pi/2$  (2-FP approach), and goes to the continuum limit by the substitution

$$c_{n\sigma} \rightarrow i^n R_\sigma(x) + (-i)^n L_\sigma(x), \quad (11)$$

where  $R_\sigma(x)$  and  $L_\sigma(x)$  describe right-moving and left-moving fermionic particles, respectively. This approach allows to treat, within the effective continuum-limit description, the gap “creating” ( $\Delta_r$  and  $U$ ) and gap “destructing” ( $t'$ ) terms on an equal footing and thus in a transparent way display the character of their competition [48].

Within the framework of the 2-FP approach the ionic ( $\Delta_r$ ) and the Hubbard ( $U$ ) terms appear as the scattering processes responsible for generation of a gap in the excitation spectrum. The staggered ionic potential introduces a single-particle backward scattering process  $H_{\Delta_r} \sim \Delta_r \int dx \sum_\sigma (R_\sigma^\dagger L_\sigma + \text{H.c.})$  and is responsible for generation of equal excitation gaps in each spin subsystem, i.e., for formation of the BI phase. The repulsive Hubbard term, via the correlated Umlapp scattering processes  $H_{\text{Umk}} \sim U \int dx (R_\uparrow^\dagger R_\downarrow^\dagger L_\uparrow L_\downarrow + \text{H.c.})$ , is responsible for the formation of the correlated Mott gap in the charge excitation spectrum.

Development of the gap in the excitation spectrum stabilizes the corresponding band and correlated insulating phases, respectively. However, since the elementary excitations in the BI and Mott insulating phases are topologically distinct, they expel each other, and at  $t' = 0$ , in the ground state of the half-filled IHM, the BI and Mott insulating phases are separated by the intermediate BOW phase [41].

Note that both of the above discussed scattering processes are intimately connected with the selected structure of the Fermi surface with two Fermi points  $\pm\pi/2$  separated by  $\pi$  and become incommensurate at any change of this condition. The “gap destructing” effect of the  $t'$  term is directly connected with a change of the commensurate structure of the Fermi surface. To maintain the half-filling and therefore to incorporate accurately the effect of the  $t'$ -term within the used 2-FP approach, one has to compensate the shift of the Fermi energy  $\delta E_F$  introduced by the  $t'$  term by a corresponding change of the chemical potential term  $\delta\mu(\mathcal{N}_\uparrow + \mathcal{N}_\downarrow)$ , where

$$\delta\mu = -\delta E_F = \begin{cases} 2t', & t' < 0.5t \\ t^2/2t', & t' > 0.5t \end{cases} \quad (12)$$

and  $\mathcal{N}_\uparrow + \mathcal{N}_\downarrow$  is the total number of electrons operator. Now, using the substitution (11) to express the n.n.n. hopping in terms of right and left fields, we obtain  $H_{t'} = -2t' \int dx \sum_\sigma (R_\sigma^\dagger R_\sigma + L_\sigma^\dagger L_\sigma) = -2t'(\mathcal{N}_\uparrow + \mathcal{N}_\downarrow)$ . and, thus the total contribution of the n.n.n. hopping term into the effective-field theory is given by the chemical potential term

$\mu_{\text{eff}}(\mathcal{N}_\uparrow + \mathcal{N}_\downarrow)$ , with [48]

$$\mu_{\text{eff}} = \begin{cases} 0 & \text{for } t' < 0.5t \\ 2t' - t^2/2t' \neq 0 & \text{for } t' > 0.5t \end{cases} \quad (13)$$

The right and left components of the Fermi fields can be bosonized in a standard way,

$$\begin{aligned} R_\sigma(x) &\rightarrow \frac{1}{\sqrt{2\pi\alpha_0}} e^{i\sqrt{4\pi}\phi_{R\sigma}(x)} \\ L_\sigma(x) &\rightarrow \frac{1}{\sqrt{2\pi\alpha_0}} e^{-i\sqrt{4\pi}\phi_{L\sigma}(x)}, \end{aligned} \quad (14)$$

where  $\phi_{R\sigma}$  ( $\phi_{L\sigma}$ ) are right(left)-moving Bose fields and  $\alpha_0$  is an infrared cutoff. We define the conjugate fields  $\phi_\sigma = \phi_{R\sigma} + \phi_{L\sigma}$  and  $\theta_\sigma = \phi_{L\sigma} - \phi_{R\sigma}$ , which possess commutation relations  $[\phi_\sigma(x), \theta_\sigma(x')] = i\pi\delta(x - x')$ . We define the charge

$$\phi_c = \frac{1}{\sqrt{2}}(\phi_\uparrow + \phi_\downarrow), \quad \theta_c = \frac{1}{\sqrt{2}}(\theta_\uparrow + \theta_\downarrow) \quad (15)$$

and spin fields

$$\phi_s = \frac{1}{\sqrt{2}}(\phi_\uparrow - \phi_\downarrow), \quad \theta_s = \frac{1}{\sqrt{2}}(\theta_\uparrow - \theta_\downarrow) \quad (16)$$

to describe corresponding degrees of freedom. After some standard algebra [6] and a rescaling of the fields, we arrive at the following bosonized version of the Hamiltonian (3):

$$\mathcal{H} = \int dx [h_s + h_c + h_{cs}], \quad (17)$$

where

$$h_s = \frac{v_s}{2} [(\partial_x \phi_s)^2 + (\partial_x \theta_s)^2] + \frac{m_s^0}{2\pi^2 a_0^2} \cos \sqrt{8\pi} \phi_s, \quad (18)$$

$$\begin{aligned} h_c &= \frac{v_c}{2} [(\partial_x \phi_c)^2 + (\partial_x \theta_c)^2] \\ &\quad - \frac{m_c^0}{2\pi^2 a_0^2} \cos \sqrt{8\pi K_c} \phi_c - \mu_{\text{eff}} \sqrt{\frac{K_c}{2\pi}} \partial_x \phi_c, \end{aligned} \quad (19)$$

$$h_{cs} = -\frac{\Delta_r}{\pi a_0} \sin \sqrt{2\pi K_c} \phi_c \cos \sqrt{2\pi} \phi_s. \quad (20)$$

Here,  $m_s^0 \sim U$  and  $m_c^0 \sim U$  are the bare values of coupling constants, the charge stiffness parameter is  $K_c < 1$  at  $U > 0$ , and  $v_s$  and  $v_c$  are velocities of spin and charge excitations.

At  $\Delta_r = 0$  the Hamiltonian (17) describes the Mott insulator-metal transition in the ground state of the half-filled Hubbard chain, caused by the change of chemical potential  $\mu_{\text{eff}}$  [34]. Respectively, at  $m_s^0 = m_c^0 = 0$ , the BI-metal transition in the ground state of the n.n. free ionic chain (see Appendix B for details). In each of these limiting cases the model reduces to the standard Hamiltonian of the sine-Gordon model with a topological term, describing the commensurate-incommensurate transition [36,37], which has been intensively studied in the past using bosonization and the Bethe ansatz [49,50]. In each case, the transition into the metallic phase takes place when the chemical potential exceeds the corresponding charge gap.

In the considered case of coupled fields with two separate sources for the charge gap formation, the situation is more complicated. To move forward let us first eliminate the chemical potential term by the gauge transformation

$$\sqrt{2\pi} \phi_c(x) \rightarrow \sqrt{2\pi} \phi_c(x) + \frac{\mu_{\text{eff}} \sqrt{K_c}}{v_c} x \quad (21)$$

and rewrite the Hamiltonian density in (17) in the following form:

$$h_s = \frac{v_s}{2} [(\partial_x \phi_s)^2 + (\partial_x \theta_s)^2] + \frac{m_s^0}{2\pi^2 a_0^2} \cos \sqrt{8\pi} \phi_s, \quad (22)$$

$$\begin{aligned} h_c &= \frac{v_c}{2} [(\partial_x \phi_c)^2 + (\partial_x \theta_c)^2] \\ &\quad - \frac{m_c^0}{2\pi^2 a_0^2} \cos(\sqrt{8\pi K_c} \phi_c + 2x/l_\mu), \end{aligned} \quad (23)$$

$$h_{cs} = -\frac{\Delta_r}{\pi a_0} \sin(\sqrt{2\pi K_c} \phi_c + x/l_\mu) \cos \sqrt{2\pi} \phi_s, \quad (24)$$

where the characteristic length

$$l_\mu = \frac{v_c}{\mu_{\text{eff}} \sqrt{K_c}} \quad (25)$$

determines the distance above which the effects of doping (i.e., deviation of the Fermi points from  $\pm\pi/2$ ) become visible. On the other hand, each of the gap-generating terms separately can be characterized by its own length scales  $l_\Delta \sim v_F/\Delta_r$ —the ionic term—and  $l_{M_c} \sim v_F/M_c$ —the Hubbard term—where  $M_c$  is the correlated charge gap.

At  $l_\mu \ll \min\{l_\Delta, l_{M_c}\}$  the gap-creating terms have strongly oscillating arguments and are wiped off upon integration, and therefore at large distances the effective theory is given by two independent Gaussian fields,

$$\mathcal{H}_i = \sum_{i=c,s} \int dx \left\{ \frac{v_i}{2} [(\partial_x \phi_i)^2 + (\partial_x \theta_i)^2] \right\}, \quad (26)$$

describing the Luttinger-liquid metallic phase with gapless charge and spin excitation spectrum. In deriving Eq. (26) we have taken into account that the perturbation caused by the cosine term in the spin channel is marginally irrelevant at  $U > 0$ . Thus, within the used 2-FP approximation, the bosonization treatment predicts the *commensurate-incommensurate* nature of both the BI-metal and metal-CI transitions.

In the opposite case, where  $l_\mu \gg \max\{l_\Delta, l_{M_c}\}$ , doping is ineffective and may be neglected. The corresponding effective-field theory coincides with that of the standard IHM [41], i.e., the theory of the two Gaussian fields in Eq. (26) coupled by the effective potential

$$\begin{aligned} V_{cs} &= \frac{M_s}{2\pi^2 a_0^2} \cos \sqrt{8\pi} \phi_s + \frac{M_c}{2\pi^2 a_0^2} \cos \sqrt{8\pi K_c} \phi_c \\ &\quad - \frac{\Delta_r}{\pi a_0} \sin \sqrt{2\pi K_c} \phi_c \cos \sqrt{2\pi} \phi_s, \end{aligned} \quad (27)$$

where  $M_c$  and  $M_s$  are considered as phenomenological parameters characterizing charge and spin gaps. In the gapped regime fluctuations of the corresponding fields are suppressed and the properties of the system are determined by the vacuum expectation values of the fields  $\phi_s$  and  $\phi_c$ , which correspond to the minimum of the potential energy in Eq. (27). Below in our analysis we follow the route developed in Ref. [41].

At weak  $U$ , where  $l_\Delta < l_\mu \ll l_{M_c}$  is the shortest length scale in the theory, the minimum of the potential energy is reached at the following two sets of minima (defined modulo  $2\pi$ ):  $\langle \phi_s \rangle = 0$ ,  $\sqrt{2\pi K_c} \langle \phi_c \rangle = \pi/2$  and  $\langle \sqrt{2\pi} \phi_s \rangle = \pi$ ,  $\langle \sqrt{2\pi K_c} \phi_c \rangle = -\pi/2$ . These sets characterize the BI phase. Indeed, in this case the alternating on-site charge density

operator

$$Q(x) = (-1)^i n_i \sim \sin \sqrt{2\pi K_c} \phi_c \cos \sqrt{2\pi} \phi_s \quad (28)$$

acquires a finite vacuum expectation value. Moreover, the vacuum-vacuum transitions,  $\Delta\phi_{s(c)} = \pm\pi$ , describe stable topological excitations carrying the charge  $Q = \Delta\phi_c/\pi = \pm 1$  and spin  $S^z = \Delta\phi_s/2\pi = \pm 1/2$  and therefore coinciding with massive single-fermion excitations of the BI.

At strong repulsion, where the large correlated (Hubbard) charge gap  $l_{M_c} < l_\mu \ll l_\Delta$  determines the shortest length scale of the system, the situation changes and each minimum in the charge sector splits into two degenerate minima:  $\langle\phi_s\rangle = 0$ ,  $\langle\sqrt{2\pi K_c}\phi_c\rangle = \phi_0, \pi - \phi_0$ , and  $\langle\sqrt{2\pi}\phi_s\rangle = \pi$ ,  $\langle\sqrt{2\pi K_c}\phi_c\rangle = -\phi_0, -\pi + \phi_0$ , where

$$\phi_0 = \arcsin(\pi \Delta_r / 2M_c).$$

These new sets of minima support, besides the CDW order, also the BOW order because for  $\langle\sqrt{2\pi K_c}\phi_c\rangle \neq \pm\pi/2$  the dimerization operator

$$\begin{aligned} \mathcal{D}(x) &= \sum_{\sigma} (-1)^n (c_{i,\sigma}^{\dagger} c_{i+1,\sigma} + \text{H.c.}) \\ &\sim \cos \sqrt{2\pi K_c} \phi_c(x) \cos \sqrt{2\pi} \phi_s(x) \end{aligned} \quad (29)$$

acquires a finite expectation value in the new vacuum. The location of the minima in the spin sector, and hence the spin quantum numbers of the topological excitations, are the same as in the BI phase. However, the charge quantum numbers become *fractional*, depending on  $\phi_0$ . The  $Z_2$  degeneracy of the spontaneously dimerized state implies the existence of topological kinks carrying the spin  $S = 1/2$  and charge  $Q = \pm 2\phi_0/\pi$  [41].

Thus, eventually, with increasing Hubbard repulsion, at  $l_\Delta \simeq l_{M_c}$  the BOW pattern is generated in the ground state. If the transition takes place at  $l_\Delta \simeq l_{M_c} < l_\mu$ , i.e., within the gapped phases, one recovers the phase diagram of the standard IHM [41]. However, if the same transition takes place at  $l_\mu < l_\Delta \simeq l_{M_c}$ , i.e., in the metallic phase, although the charge excitation spectrum is gapless, in the ground-state coexistence of the LRO CDW and BOW patterns will be present.

### C. Large $U$ spin chain limit

To complete our qualitative analysis, notice that the behavior of the spin gap substantially depends on the value of the parameter  $t'/t$ . At strong repulsion  $U \gg t, t', \Delta$  the spin degrees of freedom are described by the Hamiltonian of the frustrated Heisenberg chain

$$\mathcal{H}_{\text{Heis}} = J \sum_n \mathbf{S}_n \cdot \mathbf{S}_{n+1} + J' \sum_n \mathbf{S}_n \cdot \mathbf{S}_{n+2}, \quad (30)$$

where [51]

$$J = \frac{4t^2}{U} \left[ 1 - \frac{1}{U^2} (4t^2 - \Delta^2) \right] + \mathcal{O}(1/U^5), \quad (31)$$

$$J' = \frac{4t'^2}{U} \left[ 1 - \frac{1}{U^2} \left( \frac{4t'^4 - t^4}{t'^2} \right) \right] + \mathcal{O}(1/U^5). \quad (32)$$

Excitation spectrum of the spin chain (30) is gapless at  $J'/J < 1/4$  and gapped at  $J'/J > 1/4$  [52,53]. Consequently,

at large  $U$  and  $t' < 0.5t$  the spin excitation spectrum is gapless, while at  $t' > 0.5t$  it is gapped. Hence, at  $t' < 0.5t$  with increasing  $U$  after the appearance of the BOW phase the spin gap closing transition takes place [41], while at  $t' > 0.5t$  the spin gap remains finite in the whole area of the CI phase even at large  $U$ .

### III. NUMERICAL EXPLORATION

In order to test the validity of the picture obtained in the previous section, we investigated numerically the predicted insulator-metal-insulator transitions and relevant order parameters in the different phases. To this end we have performed DMRG [54] calculations on finite-length  $L$  chains with open boundary conditions (OBC). The employed code relies on the ITENSOR software library [55].

The parameter region of interest, as described in Sec. I, is the full range of Hubbard repulsion  $U > 0$  in the close proximity of the insulator-metal (Lifshitz) transition of the  $t$ - $t'$  ionic chain. This is achieved with  $t' \lesssim t'_c$ , where we expect to find a band insulator phase (induced by  $\Delta$  at low  $U$ ), a metallic phase at intermediate  $U$  (induced by second-neighbor hopping amplitude  $t' > 0.5t$ ), and a correlated insulator phase for large  $U$ . We found it convenient to set the energy scale as  $t = 1$ , to choose  $\Delta = 0.8$  and  $t' = 0.55$  (being  $t'_c \approx 0.638$ ), exploring the effects of Hubbard repulsion  $U$  from the noninteracting regime ( $U = 0$ ) up to large enough values to reach a Mott-like insulator, estimated as  $U \sim 4.0$ .

As the Hamiltonian  $\mathcal{H}$  in Eq. (1) commutes with the total number operator  $\mathcal{N} = \mathcal{N}_\uparrow + \mathcal{N}_\downarrow$  and the total magnetization operator  $S^z = (\mathcal{N}_\uparrow - \mathcal{N}_\downarrow)/2$ , one can compute the lower eigenvalue states of  $\mathcal{H}$  within subspaces with given quantum numbers  $N$  for the number of electrons and  $S^z$  for the total spin projection. We then denote by  $E_0(N, S^z)$  the lowest eigenvalue and by  $E_1(N, S^z)$  the first excited eigenvalue in the given subspace.

Specifically, we have focused on the following states (notice that, because of spin symmetry, reversing the sign of  $S^z$  does not change the eigenvalues):

- (1)  $N = L, S^z = 0$ , the ground state with lowest eigenvalue  $E_0(L, 0)$  and the internal excitation with first excited eigenvalue  $E_1(L, 0)$ ;
- (2)  $N = L, S^z = 1$ , the spin-flip state with lowest eigenvalue  $E_0(L, 1)$ ;
- (3)  $N = L + 1, S^z = +1/2$ , a one-particle state with lowest eigenvalue  $E_0(L + 1, 1/2)$ ;
- (4)  $N = L - 1, S^z = +1/2$ , a one-hole state with lowest eigenvalue  $E_0(L - 1, 1/2)$ ;
- (5)  $N = L + 2, S^z = 0$ , the two-particle state with lowest eigenvalue  $E_0(L + 2, 0)$ ;
- (6)  $N = L - 2, S^z = 0$ , the two-hole state with lowest eigenvalue  $E_0(L - 2, 0)$ .

These states were computed using maximal bond dimensions up to 800, the truncation error being lower than  $10^{-8}$ . However, when the energy difference between  $E_1(N, S^z)$  and  $E_0(N, S^z)$  is too small, DMRG convergence towards the ground state becomes difficult. Such difficulties indeed arose in the presumably metallic region, expected to be gapless in the thermodynamic limit, as we increased the chain length. Within our resources, for some values of  $U$ , we could not

ensure convergence for chains beyond a hundred sites. Moreover, the size-scaling behavior with inverse length  $1/L$  might change at some critical length [45], making any extrapolation technique from moderate lengths into the thermodynamic limit uncertain. We do not attempt in the present work to provide precise extrapolations. We limit ourselves to show confident finite size data, adding suggested thermodynamic extrapolations only when the scaling tendency with  $1/L$  seems stable. We find that the suggested results support the validity of our analytical predictions, as described schematically in Fig. 3.

The square of the total spin operator  $\mathcal{S} = \sum_i (c_{i,\sigma}^\dagger \frac{\sigma_{\sigma\sigma'}}{2} c_{i,\sigma'})$  also commutes with the Hamiltonian, then the total spin  $S$  is a good quantum number. However, it is not additive and can not be fixed along DMRG sweeps. We have computed, for each state obtained, the expectation value  $\langle S^2 \rangle$  to check coincidence with  $S(S+1)$  for a given integer or half-integer  $S$ .

In this sense we have found that, for any considered repulsion  $U$  and length  $L$ , the half-filled, nonmagnetized ground state is a singlet state with  $S = 0$ . The internal excitation and the spin-flip states form a triplet with  $S = 1$ . Consistently with spin symmetry, they are degenerate,  $E_1(L, 0) = E_0(L, \pm 1)$ . This is the lowest excitation of the ground state. We have found no signal of another exciton state lying below the spin triplet, in contrast with the situation observed in the nearest neighbors IHM [45].

For the ground state we have also computed the local charge and spin densities, and spin correlations along the chains, with the aim of discussing order parameters in the different phases.

We describe below the results of different measures we have performed, setting  $t = 1$ ,  $t' = 0.55$ , and  $\Delta = 0.8$ , on chains of several lengths up to 128 sites.

### A. Energy gaps

One can define different gaps with respect to the half-filled ground state, corresponding to the different possible excitations. We consider the following:

(1) the internal gap  $\Delta_{\text{int}}$  in the subspace with  $N = L$  and  $S^z = 0$ ,

$$\Delta_{\text{int}} = E_1(L, 0) - E_0(L, 0); \quad (33)$$

(2) the spin gap  $\Delta_s$  corresponding to spin-flipped states  $S^z = \pm 1$  with  $N = L$ ,

$$\Delta_s = \frac{E_0(L, 1) + E_0(L, -1) - 2E_0(L, 0)}{2}; \quad (34)$$

(3) the one-particle gap  $\Delta_1$  corresponding to the addition or subtraction of one electron,

$$\Delta_1 = E_0(L+1, 1/2) + E_0(L-1, 1/2) - 2E_0(L, 0); \quad (35)$$

(4) the two-particle gap  $\Delta_2$  corresponding to the addition or subtraction of charge while keeping the magnetization

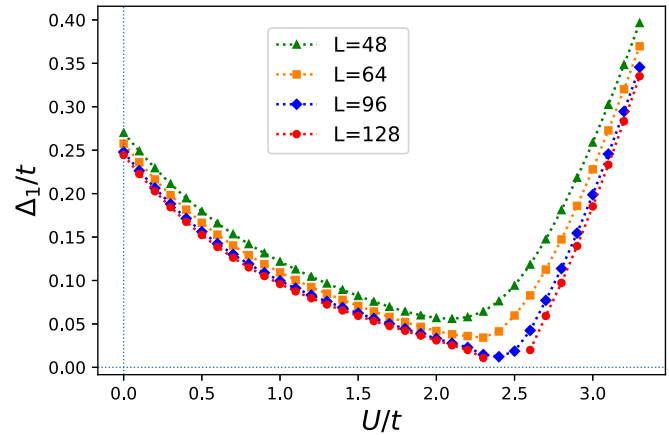


FIG. 5. One-particle gaps  $\Delta_1$ , for  $t' = 0.55t$  and  $\Delta = 0.8t$ . Data from finite chains of different lengths  $L = 48, 64, 96, 128$  is shown (some points for  $L = 128$  are not included). One can distinguish the band insulator phase for low  $U$ , signals of a gapless region for intermediate  $U$ , and a reentrance to a large  $U$  insulator phase.

$$S^z = 0,$$

$$\Delta_2 = \frac{E_0(L+2, 0) + E_0(L-2, 0) - 2E_0(L, 0)}{2}. \quad (36)$$

Notice that a chemical potential should be added to ensure that the half-filling  $N = L$  sector contains the ground state of the system. However, chemical potential contributions cancel out in these gap constructions, then gaps can be computed directly from the eigenvalues of the Hamiltonian in Eq. (1).

From the degeneracy of the spin triplet one can see that  $\Delta_{\text{int}} = \Delta_s$ . Moreover, the present definition of the spin gap coincides with the difference between the triplet and singlet energies at half-filling [ $E(N = L, S = 1) - E(N = L, S = 0)$ ] used elsewhere. From the same relation, as there is no exciton state below the spin gap, we assume that  $\Delta_2$  is a meaningful measure of the charge gap. We denote  $\Delta_2$  as  $\Delta_c$  in the following.

We first show in Fig. 5 the one-particle gap  $\Delta_1$ , which involves the change of both charge and spin quantum numbers. The key feature of this plot is the apparent presence of a gapless region for intermediate  $U$ . Notice that some points for  $L = 128$  with convergence difficulty are not included; in these cases the gap seems to be so small that our procedures have not been able to separate the ground state from the first excited level.

In order to analyze separately charge and spin degrees of freedom, we show in Fig. 6 the two-particle charge gap  $\Delta_c$  ( $\Delta_2$ ). As expected for finite systems [45], we observed that  $\Delta_c > \Delta_1$ . The existence of a gapless region at intermediate  $U$ , in the thermodynamic limit, is not evident from the largest length studied and requires a detailed size scaling analysis. In Fig. 7 we show that the  $1/L$  scaling behavior is very different at low, mid, or large  $U$ . A power law  $L^{-\nu}$  in the BI phase, and a quadratic polynomial in the CI phase, fit well the finite size data providing the suggested extrapolation in Fig. 6 (in gray). However, in the region  $2.2 \lesssim U \lesssim 2.7$  it is apparent that larger sizes are needed to define  $1/L$  scaling. Though we do not propose an extrapolation, a graphical inspection suggests the presence of the unusual gapless phase in this region.

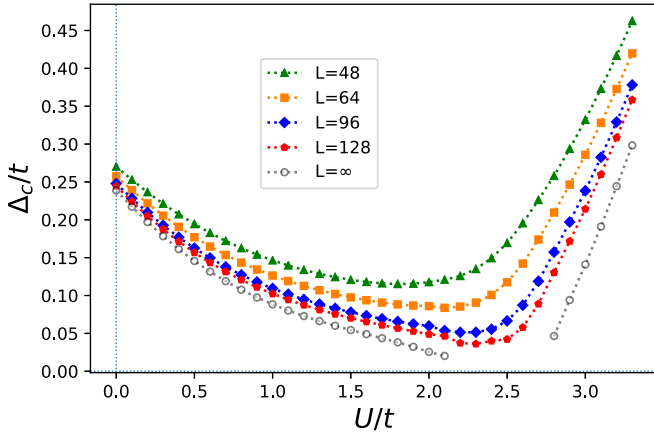


FIG. 6. Two-particle charge gap  $\Delta_c$ , for  $t' = 0.55t$  and  $\Delta = 0.8t$ . Data from finite chains of different lengths  $L = 48, 64, 96, 128$  is shown, together with a proposed extrapolation where appropriate (hollow circles). The band insulator phase for low  $U$  and the correlated insulator phase for large  $U$  can be distinguished. At intermediate  $U$  the lengths computed do not provide a definite scaling tendency; we argue in Fig. 7 that our data is consistent with a gapless thermodynamic limit.

Next we show in Fig. 8 the spin gap  $\Delta_s$ , coincident with the internal excitation gap in the half-filled, nonmagnetized subspace of states. Being the lowest excitation of the ground state, we have not reached good DMRG convergence in the  $2.2 \leq U \leq 2.7$  region where the internal excitation could not be separated from the ground state. From the available data we show in Fig. 9 the scaling tendency. One finds a finite spin gap in the band insulator region, a possibly spin gapless phase in the intermediate region, and a reopening of the spin gap in the correlated insulator region. In this last region we observed a regular scaling behavior that leads to a sensible mathematical extrapolation: a quadratic fit provides a small but nonvanishing, decaying, spin gap in the thermodynamic limit (shown in the inset). This is consistent with the spin dimerized phase predicted in Sec. II C. The suggested extrapolation is plotted in Fig. 8 (in gray). Further investigation, exceeding our numerical resources, is needed in the intermediate region.

From the shown data one can infer for low  $U$  a band insulator type region (BI, noncorrelated) with (almost)  $\Delta_c = \Delta_s$ . The gaps decay as the repulsion  $U$  penalizes double occupation of low-potential (odd) sites and promotes n.n.n. hopping  $t'$  between high-potential (even) sites. The charge gap  $\Delta_c$  and the spin gap  $\Delta_s$  presumably close at  $U_{c,1} \approx 2.2$  (we cannot resolve whether they would close at the same point), giving rise to the repulsion-driven metallic phase. When larger repulsion  $U$  gets strong enough to also penalize double occupation of high-potential sites, the charge gap reopens and starts to grow with  $U$ . This occurs at  $U_{c,2} \approx 2.7$ . It is expected that the charge gap increases linearly in this region, from the fact that our computations are done with a fixed number of particles instead of fixing the chemical potential (see Ref. [56] and Appendix B for a discussion). Interestingly, the spin gap also reopens close to  $U_{c,2}$ , and grows to a maximum in a narrow range of  $U$ , as if bound to the charge gap. This unusual behavior seems not to be captured by the 2-FP bosonization

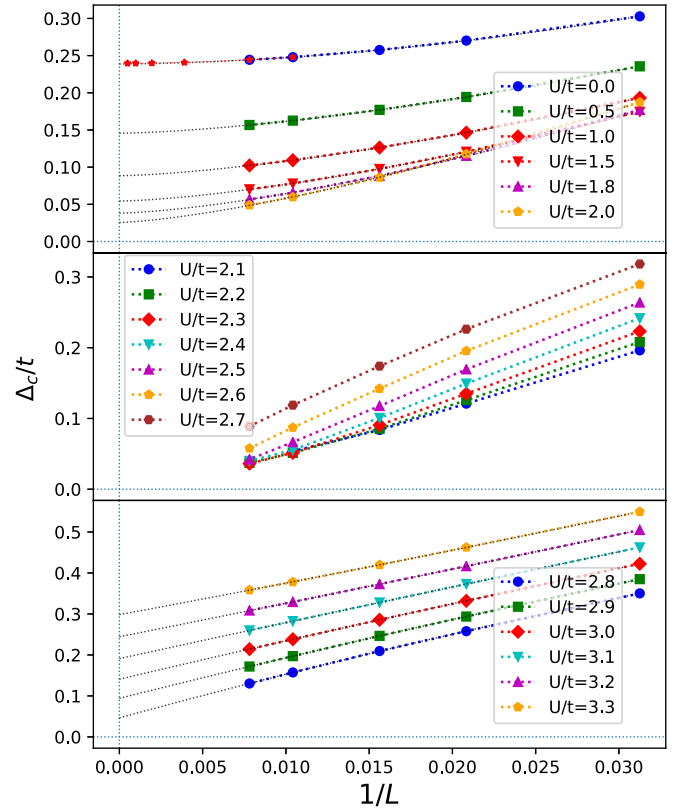


FIG. 7. Finite size scaling of the charge gap for different values of the Hubbard repulsion, with  $L$  ranging from 32 to 128 sites. An extrapolation is shown as a guide to the eye when appropriate. Top panel: for low  $U$  the charge gap scaling can be fitted with a power law  $\Delta_c(\infty)/t + L^{-\nu}$ , and clearly extrapolates towards a nonzero band insulator gap (for  $U = 0$  we added large size free-electron results, in red stars). Middle panel: in the intermediate region the scaling concavity changes from positive to negative. A naive extrapolation from our finite size data is misleading, meaning that there should be a change in the scaling tendency at larger lengths. Though refined computations are needed, a graphical inspection strongly suggests that the present results are consistent with a gapless thermodynamic limit. Bottom panel: for larger  $U$  the negative scaling concavity smoothly gives place to a polynomial behavior. For  $U \geq 2.8t$  a quadratic extrapolation is again clearly nonzero, corresponding to the correlated (Mott-like) insulator phase.

approach in Sec. II B. Beyond a peak value at  $U \approx 2.80$  the spin gap starts to decay while the charge gap keeps growing, signaling a strongly correlated insulator phase. In order to investigate the role of the ionicity  $\Delta$  in the gap formation, we have additionally explored the range  $0 \leq \Delta \leq 0.9$ , keeping  $t = 1$  and  $t' = 0.55$  close to the Lifshitz point. Without reaching further numerical precision, we have observed that when the ionic potential amplitude  $\Delta$  is lower, the argued metallic region starts at lower  $U_{c,1}$  and is eventually present since the free point  $U = 0$  when  $\Delta$  is low enough. The value of  $U_{c,2}$  where the charge gap reopens is less sensitive to the ionicity. The spin gap peak close to  $U_{c,2}$  was observed for any  $\Delta$ . An estimation of the transition points according to the ionicity parameter is shown in Fig. 10.

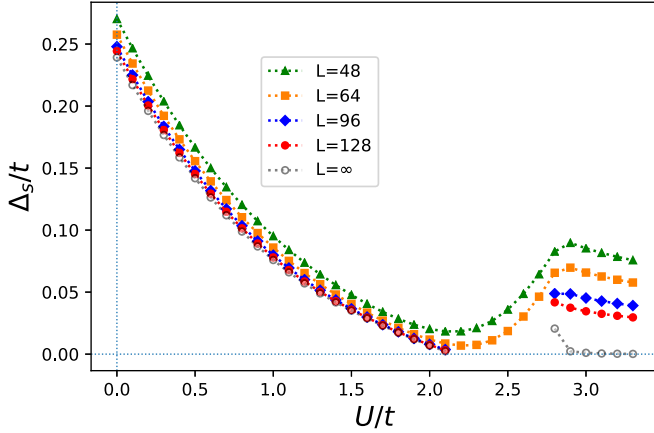


FIG. 8. Spin gap  $\Delta_s$ , for  $t' = 0.55t$  and  $\Delta = 0.8t$ . Data from finite chains of different lengths  $L = 48, 64, 96, 128$  is shown only where DMRG convergence is reached. The band insulator phase for low  $U$  with similar spin and charge gaps can be distinguished. The correlated insulator phase for large  $U$  shows a rise of the spin gap followed by a slow decay. An extrapolation is shown when appropriate (hollow circles, see details in Fig. 9).

## B. Order parameters

For the computed ground states we have evaluated the local expectation values  $\rho_{i,\sigma} = \langle n_{i,\sigma} \rangle$  for each site and  $q_{i,\sigma} = \langle c_{i,\sigma}^\dagger c_{i+1,\sigma} + \text{H.c.} \rangle$  for each bond, as well as spin-spin correlations  $\langle S_i^z S_j^z \rangle$ , with the aim of revealing the existence of magnetic order. The following local densities are then considered:

- (1) local charge density  $\rho_i = \rho_{i,\uparrow} + \rho_{i,\downarrow}$ ;
- (2) bond charge density  $q_i = q_{i,\uparrow} + q_{i,\downarrow}$ .

The local spin density  $\sigma_i = \frac{1}{2}(\rho_{i,\uparrow} - \rho_{i,\downarrow})$  and the bond spin density  $q_{i,\uparrow} - q_{i,\downarrow}$  do vanish, as expected from the  $SU(2)$  symmetry of the model and the zero magnetization condition.

### 1. Charge density wave

Our results for the induced CDW order (ionicity) are summarized in Fig. 11. Local charge density  $\rho_i$  is found to be alternating around the half-filling average  $\bar{\rho}_i = 1$ , following the pattern induced by ionic potential. According to Eq. (1), even sites have higher local potential so they are less occupied by electrons. We show in the inset the charge density in the central portion of a chain sample ( $U = 2.5$ ,  $L = 96$ , gapless region) to illustrate the CDW order. A similar alternating pattern is observed in the band insulator and correlated insulator phases; boundary effects disappear in a few sites and the occupation alternation gets homogeneous in the bulk.

The CDW amplitude for chains of length  $L$  was then computed as

$$\delta\rho = \frac{1}{L} \sum_{i=1}^L (-1)^{i+1} \rho_i, \quad (37)$$

comparing the occupation of odd and even sites along the chains. According with the short range of boundary effects, we found that the finite size scaling is linear in  $1/L$ . These results provide full support for the mean-field approach developed in Sec. II A and are in concordance with the mean-field

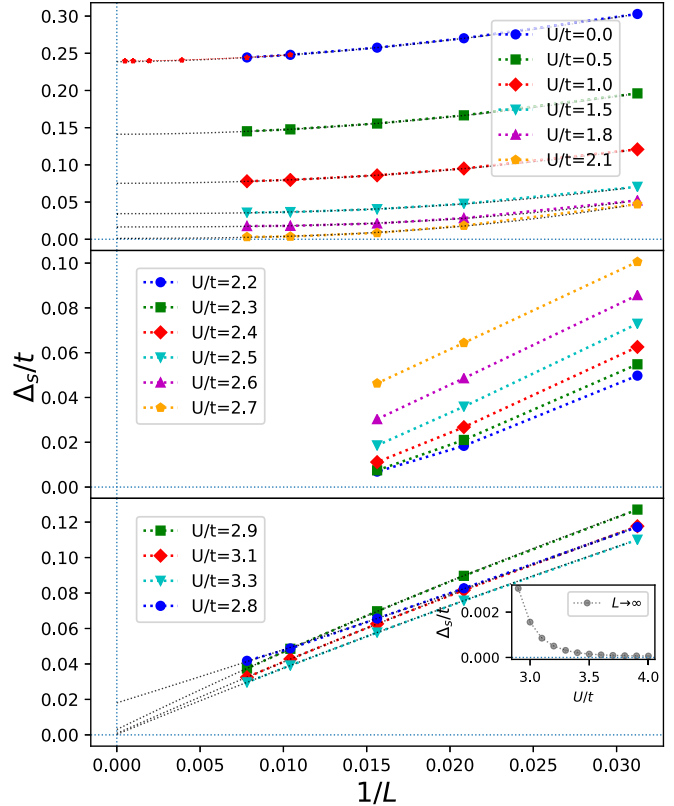


FIG. 9. Finite size scaling of the spin gap for different values of the Hubbard repulsion, with  $L$  ranging from 32 to 128 sites. Top panel: for low  $U$  a power law scaling of the spin gap suggests nonzero extrapolations, with values similar to the charge gap (for  $U = 0$  large size free-electron results are also shown, in red stars). The extrapolated spin gap decreases smoothly with  $U$ , while the scaling maintains the slope and concavity. We estimate that it is nonzero up to  $U \approx 2.1t$ . Middle panel: in the intermediate region the scaling looks almost linear, but a naive extrapolation would lead to meaningless results; this means that for larger lengths there should be a crossover in the scaling tendency. Though we have not reached DMRG convergence for larger systems in this region, the behavior might be compatible with a gapless thermodynamic limit up to  $U \approx 2.7t$ . Bottom panel: a singular behavior is observed at  $U = 2.8t$ , where the spin gap reopens and gets a peak value. For higher  $U \geq 2.9t$  the scaling gets a slight negative concavity and a quadratic extrapolation decreases smoothly towards zero. Inset: a quadratic extrapolation in this region suggests nonvanishing, decaying, spin gaps.

parameter  $\delta\rho_0$  defined in Eq. (2). We show in the main panel of Fig. 11 the finite size values of  $\delta\rho$  and the corresponding extrapolation. It is clear that  $\delta\rho$  decreases with  $U$ , as the Hubbard repulsion penalizes local occupation larger than one [cf. the mean field  $\delta\rho_0(U)$  in Fig. 4].

### 2. Bond-ordered wave

In the thermodynamic limit the Hamiltonian in Eq. (1) is symmetric under reflection with respect to a site. This implies that all bonds are equivalent, and one expects that the bond charge density  $q_i$  should be homogeneous. However, a spontaneous parity symmetry breaking is known to occur in the

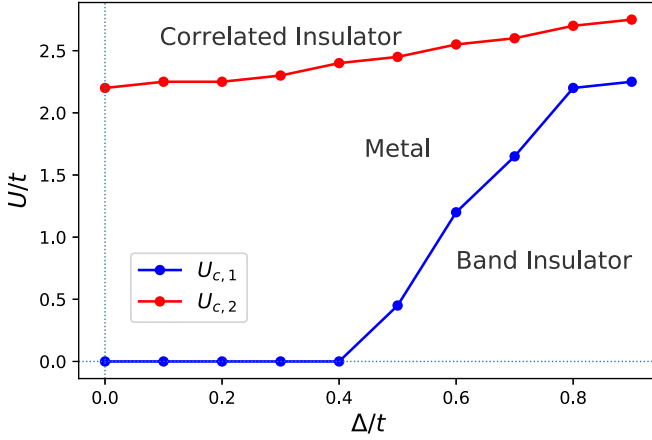


FIG. 10. Estimated transition points for different ionicities  $\Delta$  and  $t' = 0.55t$ .  $U_{c,1}$  corresponds to the band insulator-metal transition where the charge gap vanishes, and  $U_{c,2}$  to the metal-correlated insulator transition where the charge gap reopens.

( $t' = 0$ ) IHM at intermediate repulsion  $U$  [41,45], manifest as a BOW phase with a twofold degenerate, dimerized ground state characterized by alternating bond charge density  $q_i$ . We address in this section the appearance of such a BOW phase in the  $t$ - $t'$  ionic Hubbard model.

The use of OBC in the ionic chain with even number of sites  $L$  explicitly breaks the reflection symmetry, as the edge sites have different ionic potential  $\pm\Delta/2$ . This induces an alternation of  $q_i$ , as shown in sample plots in the inset of Fig. 12. One then has to distinguish the true BOW order in the bulk from the oscillating boundary effects. To this end we have evaluated the average oscillation amplitudes of  $q_i$  in the ground state of finite-length chains as

$$\text{BOW} = \frac{1}{L-1} \sum_{i=1}^{L-1} (-1)^i q_i, \quad (38)$$

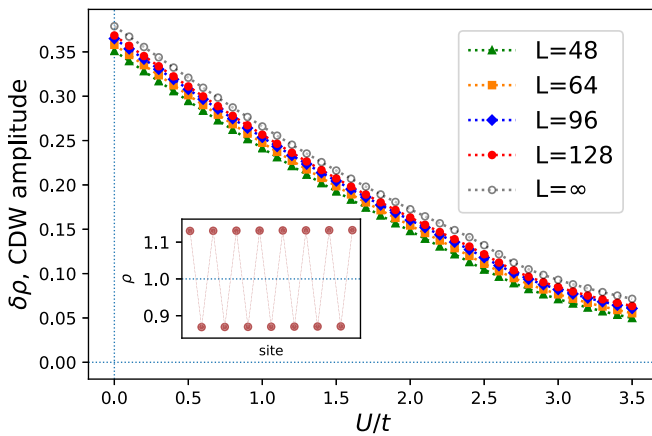


FIG. 11. The amplitude of local charge density alternation  $\delta\rho$  decreases smoothly with  $U$ . Data is averaged along chains of length  $L = 48, 64, 96, 128$  and extrapolated linearly in  $1/L$ . Notice that the slope is slightly different in the metallic region. Inset: detail of the CDW in a portion of a chain sample ( $L = 96$  sites) for  $U = 2.5t$  in the metallic phase; the same alternating occupation pattern is observed for all  $U$ .

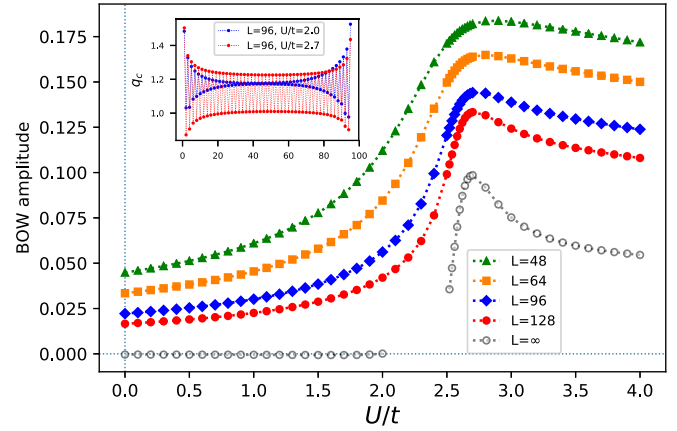


FIG. 12. Average BOW amplitude for finite-length chains with  $L$  ranging from 48 to 128 sites. Extrapolation to the thermodynamic limit is only suggested (hollow circles) where the scaling tendency is well defined (see Fig. 13). No bond order is present in the BI phase but a BOW amplitude appears and increases rapidly within the metallic phase ( $U \geq 2.52t$  is shown), then decreases slowly in the CI phase. Inset: samples of the charge bond density in a chain of length  $L = 96$  sites with OBC. The density oscillates and the difference between odd and even bonds is always enhanced at the end bonds; for the shown  $U = 2.0t$  the amplitude decays to zero towards the chain center but for  $U = 2.7t$  it decays to a finite steady value that signals the bulk BOW order in the  $L \rightarrow \infty$  limit.

and then studied their scaling behavior with  $1/L$ . In Fig. 12 we show the finite size BOW amplitudes for a wide range of  $U$  and suggest the extrapolated values where we find them trustworthy, from the analysis of the scaling behaviors provided in Fig. 13. In the BI phase the behavior is linear, leading to the absence of BOW order. Our present data is not enough to resolve the scaling behavior in the intermediate region, where the curvature cannot be clearly fitted. Starting within the gapless region, and extending into the correlated insulator phase, a quadratic extrapolation clearly indicates BOW order. From this analysis we suggest that the BOW order starts at some  $U_c^*$  located between 2.5 and 2.6, and has a peak value where the charge gap reopens. Such a profound manifestation within the charge and spin gapless phase of the corresponding quantum phase transition at  $U_c^*$  makes this metallic state highly unusual. This main result is indicated in the schematic phase diagram in Fig. 3.

The BOW order remains present in the CI phase, with an amplitude that decreases with  $U$ . As discussed in Sec. II B, we do expect this remnant BOW order, as in the large  $U$  limit the Hamiltonian in Eq. (1) can be mapped onto a  $J$ - $J'$  spin  $S = 1/2$  Heisenberg model with large enough  $J' > J/4$  as to be in the dimerized regime.

### 3. Spin dimerization and antiferromagnetic order

As the expectation values of spin components vanish at every site, the magnetic order is investigated by means of the correlation functions  $\langle S_i^z S_j^z \rangle$  with

$$S_i^z = (c_{i,\uparrow}^\dagger c_{i,\uparrow} - c_{i,\downarrow}^\dagger c_{i,\downarrow})/2. \quad (39)$$

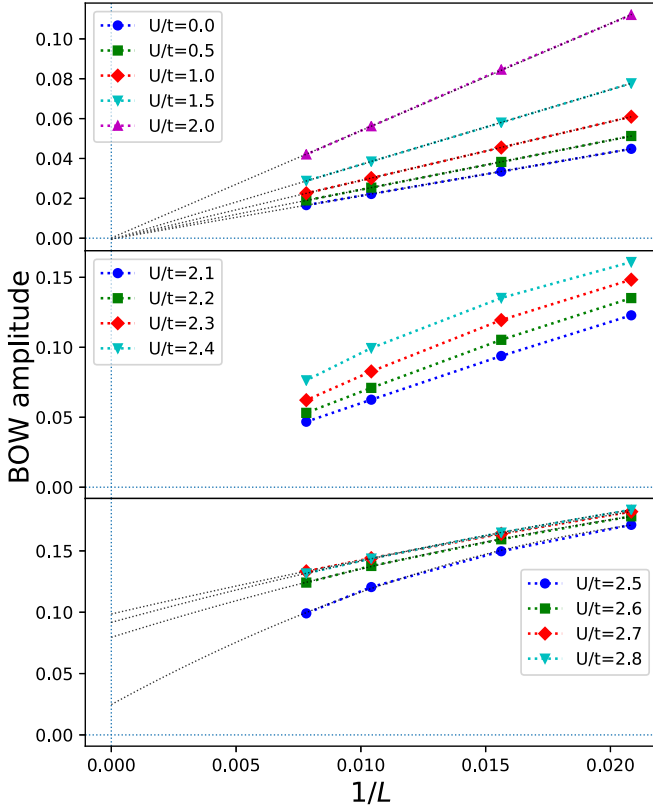


FIG. 13. BOW amplitude scaling. We show the finite size BOW amplitudes in different regions of the Hubbard repulsion, and their suggested extrapolations when trustworthy. Top panel: the average along the chains includes important boundary effects that in the BI phase extrapolate linearly to zero. There is no bond order in this phase. Middle panel: in the metallic phase, up to  $U = 2.5t$  the scaling behavior is not well defined from the computed lengths. No extrapolation is done. Bottom panel: starting at  $U = 2.5t$ , within the metallic phase, a quadratic extrapolation leads to nonzero BOW amplitude. Still, the scaling behavior at  $U = 2.5t$  might change for larger lengths. A maximum is reached at  $U \approx 2.7t$ , presumably coinciding with  $U_{c,2}$  at the onset of the charge gap.

On general grounds, the Hubbard repulsion  $U > 0$  induces antiferromagnetic correlations. The nearest-neighbor spin correlations  $\langle S_i^z S_{i+1}^z \rangle$  might be expected to be homogeneous in the thermodynamic limit because of the site reflection symmetry; however, spontaneous spin dimerization is known to occur in antiferromagnetic  $J$ - $J'$  spin chains [52,53]. The n.n.n. hopping terms  $t'$  in the present model introduce antiferromagnetic n.n.n. spin couplings that could induce such an effect. In order to detect spin dimerization in the ground state, we define a n.n. spin correlation wave (SCW) order parameter

$$\text{SCW} = -\frac{1}{L-1} \sum_{i=1}^{L-1} (-1)^i \langle S_i^z S_{i+1}^z \rangle. \quad (40)$$

The use of OBC conditions in finite chains explicitly breaks the reflection symmetry and induces oscillations of the n.n. spin correlations. In analogy with the discussion of the BOW order, we have followed a scaling analysis to separate bulk from boundary contributions. It suggests a clear thermody-

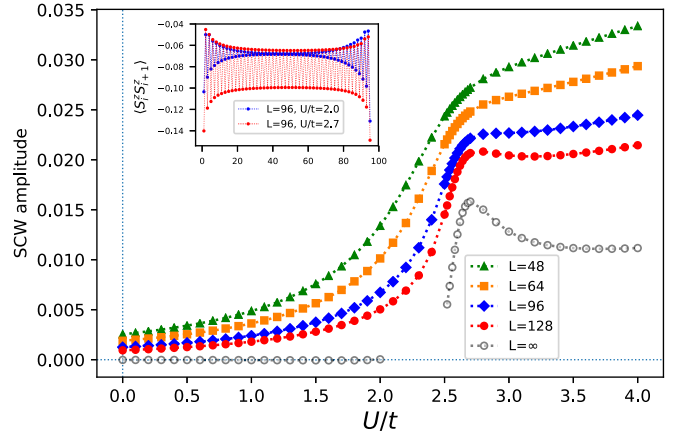


FIG. 14. Spin dimerization order parameter SCW for finite-length chains with  $L$  ranging from 48 to 128 sites. Extrapolation to the thermodynamic limit is only suggested (hollow circles) where the scaling tendency is well defined. Spin dimerization is absent in the BI phase but appears within the gapless phase, with a peak amplitude roughly where the correlated charge gap opens. Inset: profiles of local correlations  $\langle S_i^z S_{i+1}^z \rangle$  for values of  $U$  in the BI phase and at the metal-CI transition, both for  $L = 96$  sites chains.

dynamic limit for low and high values of  $U$  but does not provide a well-defined scaling tendency in the intermediate region. Our finite size results and the suggested extrapolation, where confident, are shown in Fig. 14; the inset illustrates the presence (or absence) of the SCW in the bulk. The results support that the spin dimerization takes place within the gapless phase, with a peak amplitude where the correlated charge gap opens. By comparing with Fig. 12 it is apparent that the BOW order and the spin dimerization belong together.

Farther neighbors spin-spin correlations decay with distance. The observed decay rate is compatible with an exponential behavior in the BI phase, with a correlation length of a few sites that increases as the spin gap decreases with

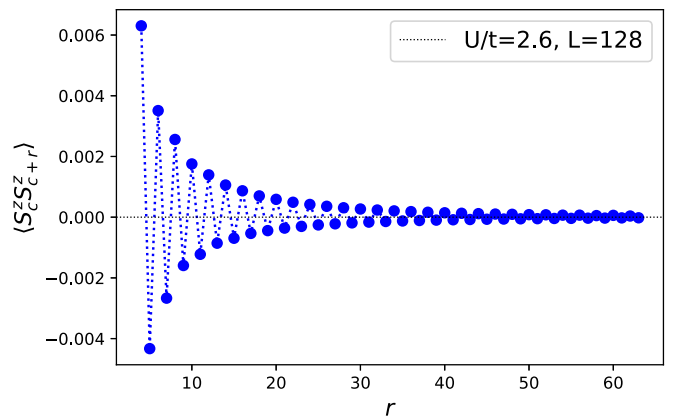


FIG. 15. Large distance spin correlations  $\langle S_c^z S_{c+r}^z \rangle$ , where  $c = L/2$  is a central site in a  $L = 128$  sites chain, for  $U = 2.6$  in the metallic region. An antiferromagnetic order is present, but it is hard to distinguish whether correlations follow an exponential decay with large correlation length or an inverse distance power law.

larger  $U$ . In the CI phase our data is compatible with a quasi-long-range antiferromagnetic order, with alternate correlations decaying like an inverse distance power law; this is consistent with the mapping into a  $J$ - $J'$  Heisenberg spin chain discussed in Sec. II B and the very small spin gap discussed in Sec. III A. In the intermediate metallic region we observe the formation of a short-range antiferromagnetic order, as illustrated in Fig. 15 in a chain of  $L = 128$  sites for  $U = 2.6$ . The decay rate presumably undergoes a crossover from exponential, with a large correlation length, into a quasi-long-range order.

#### IV. SUMMARY AND CONCLUSIONS

In the present work we investigate the ground state of an extended one-dimensional ionic Hubbard model with nearest-neighbors hopping  $t$ , next-to-nearest-neighbors hopping  $t'$ , ionic potential  $\Delta$ , and Hubbard on-site repulsion  $U$ , setting  $t'$  in an intermediate regime where previous studies [47] have not been conclusive. We restrict the analysis to half-filling and zero magnetization states.

We have focused on a fixed value of  $t'$  and  $\Delta$ , where the free  $t$ - $t'$ - $\Delta$  chain is still an indirect gap insulator, close to the would-be Lifshitz transition if  $\Delta$  was absent. Then, we investigate the effects of the Hubbard repulsion. Numerically, we set  $t' = 0.55t$  and  $\Delta = 0.8t$ . Because for the selected set of model parameters the low-energy physics of the noninteracting particles is given by excitations with nonlinear dispersion, it is a challenge to analyze the effect of electron-electron interactions  $U$  on the system.

On the analytical side we have followed a bosonization approach starting from the free fermion system, with two commensurate Fermi momenta. As  $t' > 0.5t$  shifts the Fermi points, a chemical potential is introduced to reestablish them so that perturbations due to  $\Delta$ ,  $U$ , and  $t'$  can be treated on equal footing. It comes out that three independent length scales determine the behavior of the ground state: one associated with the renormalized ionic gap, one associated with the Hubbard correlated gap, and a third one associated with the chemical potential. When the chemical potential exceeds the ionic and correlated gaps, the metallic phase is established by means of a commensurate-incommensurate transition. Features of the standard IHM, such as the appearance of the BOW order and dominance of correlations, occur within this metallic phase while the charge gap remains zero. Instead, when the ionic gap or the correlated gap (excluding each other) become larger than the effective chemical potential, the band insulator or the correlated insulator phases, respectively, are formed. These findings can be qualitatively appreciated in Fig. 16, where we compare the charge gap obtained for the IHM ( $t' = 0$ ) with the chemical potential due to  $t' > 0.5t$ .

On the numerical side we have explored a wide range of  $U$  using the DMRG technique. We show that the Hubbard repulsion competes with the ionic free electron state, reducing the charge gap. Though a vanishing gap makes it difficult to separate the ground state from excitations, our finite size results suggest that the Hubbard repulsion drives the system into a gapless ground state at some critical point  $U_{c,1}$ . This is reminiscent of the so-called interaction-resistant metals [57].

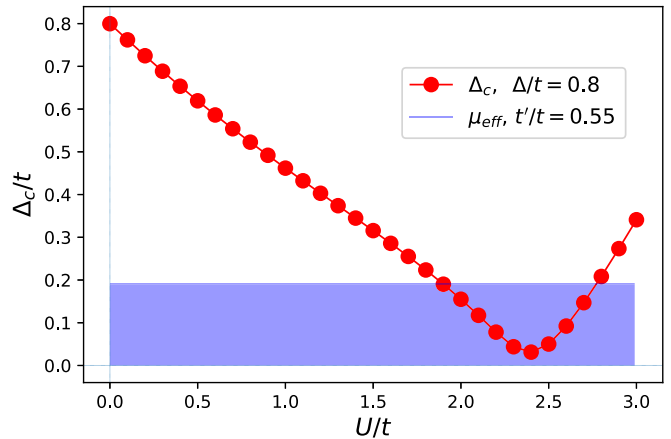


FIG. 16. Qualitative argument comparing the charge gap for the standard IHM ( $\Delta = 0.8t$ ,  $t' = 0$ , rough DMRG computation in red circles) and the chemical potential introduced by  $t' > 0.5t$  in the bosonization approach (for  $t' = 0.55t$ ). When the  $t' = 0$  charge gap is lower than the effective Fermi level (blue surface), fluctuations dominate and the metallic state is stabilized. Spontaneous generation of the BOW order occurs inside the metallic phase, making it highly unusual. The estimated boundaries of the insulator phases in Fig. 6 are compatible with this simple picture.

The gapless state is alleged to persist in a wide window of  $U_{c,1} < U < U_{c,2}$ , with neither charge gap nor spin gap and with a long-range order CDW pattern induced by the ionic potential. After a critical point  $U_c^*$  ( $U_{c,1} < U_c^* < U_{c,2}$ ) the state also supports short-range antiferromagnetic order, spontaneous charge bond order, and nearest-neighbors spin correlation dimerization. These features characterize a very unusual metallic state.

Larger repulsion gives rise to a correlated insulator (Mott-like) phase at some critical point  $U_{c,2}$ . The charge gap opens linearly with  $U$ , while the spin gap also opens slightly after  $U_{c,2}$ , showing a small peak to decay later presumably not closing at any  $U$ . The CDW and the BOW, with decaying amplitude, coexist with quasi-long-range antiferromagnetic order in this correlated insulator phase.

Additional analytical insight is obtained for large  $U$  by freezing the charge degrees of freedom at one electron per site, thus mapping the model into a spin  $S = 1/2$  Heisenberg  $J$ - $J'$  chain. As one gets  $J'/J > 1/4$ , the spin system lays in the dimerized phase. This explains the persistence of the BOW order and the finite  $1/U$  spin gap within the explored range of  $U$ .

We expect that the present predictions could be traced in fermionic cold-atom systems in suitable engineered optical lattices.

#### ACKNOWLEDGMENTS

G.I.J. acknowledges A. A. Nersesyan, M. Sekania, and S. Garuchava for many useful discussions. This work was partially supported by CONICET (Grant No. PIP 2021-1146), Argentina, and the Shota Rustaveli National Science Foundation of Georgia, SRNSF, Grant No. FR19-11872.

**APPENDIX A: DIAGONALIZATION OF THE IONIC CHAIN**

In this Appendix we consider the exactly solvable case of the  $t$ - $t'$  ionic chain given by the Hamiltonian

$$\begin{aligned} \mathcal{H}_{t-t'-\Delta_r} = & -t \sum_{i,\sigma}^L (c_{i,\sigma}^\dagger c_{i+1,\sigma} + \text{H.c.}) \\ & + t' \sum_{i,\sigma}^L (c_{i,\sigma}^\dagger c_{i+2,\sigma} + \text{H.c.}) \\ & + \frac{\Delta_r}{2} \sum_{i,\sigma}^L (-1)^i n_{i,\sigma}. \end{aligned} \quad (\text{A1})$$

To diagonalize the Hamiltonian (A1) it is convenient to introduce a unit cell with two sites and operators

$$a_{m,\sigma} \equiv c_{2m-1,\sigma}, \quad b_{m,\sigma} \equiv c_{2m,\sigma}, \quad m = 1, \dots, L/2$$

and rewrite the reduced version of the Hamiltonian in the following way:

$$\begin{aligned} \mathcal{H}_{t-t'-\Delta_r} = & -t \sum_{m,\sigma} [a_{m,\sigma}^\dagger (b_{m,\sigma} + b_{m-1,\sigma}) + \text{H.c.}] \\ & + t' \sum_{m,\sigma} [a_{m,\sigma}^\dagger a_{m+1,\sigma} + b_{m,\sigma}^\dagger b_{m+1,\sigma} + \text{H.c.}] \\ & - \frac{\Delta_r}{2} \sum_{m,\sigma} (n_{m,\sigma}^{(a)} - n_{m,\sigma}^{(b)}), \end{aligned} \quad (\text{A2})$$

where  $n_{m,\sigma}^{(a)} = a_{m,\sigma}^\dagger a_{m,\sigma}$ ,  $n_{m,\sigma}^{(b)} = b_{m,\sigma}^\dagger b_{m,\sigma}$  are spin  $\sigma$  particle density operators on odd ( $a$ ) and even ( $b$ ) sites, respectively.

Performing the Fourier transformation

$$\begin{aligned} a_{m,\sigma} &= \sqrt{\frac{2}{L}} \sum_k e^{ikm} a_{k,\sigma}, \\ b_{m,\sigma} &= \sqrt{\frac{2}{L}} \sum_k e^{ik(m+\frac{1}{2})} b_{k,\sigma}, \end{aligned} \quad (\text{A3})$$

where  $k = \frac{4\pi}{L}\nu$ , with integer  $\nu$ ,  $-\frac{L}{4} < \nu \leq \frac{L}{4}$ , and introducing a two-spinor

$$\Psi^\dagger = (a_{k,\sigma}^\dagger, b_{k,\sigma}^\dagger), \quad \Psi = \begin{pmatrix} a_{k,\sigma} \\ b_{k,\sigma} \end{pmatrix}, \quad (\text{A4})$$

we rewrite the Hamiltonian in momentum space as

$$\mathcal{H}_{t-t'-\Delta_r} = \Psi^\dagger \hat{\mathcal{H}} \Psi, \quad (\text{A5})$$

where

$$\hat{\mathcal{H}} = \varepsilon'_k \mathbb{I} + \varepsilon_k \hat{\tau}_x - \frac{1}{2} \Delta_r \hat{\tau}_z, \quad (\text{A6})$$

$$\varepsilon_k = -2t \cos \frac{k}{2}, \quad \varepsilon'_k = 2t' \cos k, \quad (\text{A7})$$

$\mathbb{I}$  is an identity matrix, and  $\hat{\tau}_x$  and  $\hat{\tau}_z$  are Pauli matrices. Diagonalization of the Hamiltonian in the form (A6) is straightforward. The Bogolyubov transformation

$$\begin{aligned} a_{k,\sigma} &= \cos \varphi_k \alpha_{k,\sigma} + \sin \varphi_k \beta_{k,\sigma}, \\ b_{k,\sigma} &= -\sin \varphi_k \alpha_{k,\sigma} + \cos \varphi_k \beta_{k,\sigma}, \end{aligned} \quad (\text{A8})$$

where the angles  $\varphi_{k,\sigma}$  are chosen as

$$\tan 2\varphi_k = \frac{2\varepsilon_k}{\Delta_r}, \quad \cos 2\varphi_{k,\sigma} = \frac{\Delta_r}{\sqrt{4\varepsilon_k^2 + \Delta_r^2}}, \quad (\text{A9})$$

diagonalizes the Hamiltonian (A5) as

$$\mathcal{H}_{t-t'-\Delta_r} = \sum_{k,\sigma} (E_k^- \alpha_{k,\sigma}^\dagger \alpha_{k,\sigma} + E_k^+ \beta_{k,\sigma}^\dagger \beta_{k,\sigma}), \quad (\text{A10})$$

where

$$E_k^\pm = \varepsilon'_k \pm \sqrt{\varepsilon_k^2 + (\Delta_r/2)^2} \quad (\text{A11})$$

are the energy dispersions for  $\alpha$  and  $\beta$  quasiparticles, respectively.

In the ground state of the half-filled system the  $L$  lowest-energy states are filled and the rest are empty. For  $t' = 0$ ,  $E_k^-$  and  $E_k^+$  do not overlap and are separated with a direct gap equal to  $\Delta_r$ ; all states in the lower band are occupied, whereas in the upper band all states are empty; the system is in the insulating state. In the case of a finite  $t'$ , however, these bands might overlap, due to a  $k$ -dependent energy shift  $\varepsilon'_k$ . For  $t, t' > 0$  the global minimum of the upper  $E_k^+$  band is always at  $k = \pi$ ,

$$E_{k=\pi}^+ = -2t' + |\Delta_r|/2. \quad (\text{A12})$$

The  $E_k^-$  (lower) band shows a richer composition of maxima: at

$$t'_* = 0.5t \sqrt{1 + (\Delta_r/4t)^2} - |\Delta_r|/8, \quad (\text{A13})$$

the position of the global maximum of the lower band is changed from  $k = \pi$ ,  $E_{k=\pi}^- = -2t' - |\Delta_r|/2$  ( $t' < t'_*$ ), to  $k = 0$ ,  $E_{k=0}^- = 2t' - 2t \sqrt{1 + (\Delta_r/4t)^2}$  ( $t' > t'_*$ ). These possibilities are illustrated in Fig. 2 in the main text.

Hence, for  $t' < t'_*$ , the system is a band insulator with a direct gap in the excitation spectrum

$$\Delta_{\text{dir}} = E_{k=\pi}^+ - E_{k=\pi}^- = |\Delta_r|, \quad (\text{A14})$$

while for  $t'_* < t' < t'_c$ , where

$$t'_c = 0.5t \sqrt{1 + (\Delta_r/4t)^2} + |\Delta_r|/8 \quad (\text{A15})$$

is an insulator with the indirect gap

$$\Delta_{\text{ind}} = |\Delta_r|/2 + 2t \sqrt{1 + (\Delta_r/4t)^2} - 4t' \quad (\text{A16})$$

in the excitation spectrum. The gap decreases linearly with increasing  $t'$  and vanishes at  $t' = t'_c$ . It is useful to reverse the problem and determine the critical value of the effective ionicity parameter  $\Delta_r^{\text{cr}} \geq 0$  corresponding to the metal-insulator transition at given values of the parameters  $t$  and  $t'$ ,

$$\Delta_r^{\text{cr}} = \begin{cases} 4t' - t^2/t' & \text{for } t' \geq 0.5t \\ 0 & \text{otherwise} \end{cases}. \quad (\text{A17})$$

For  $|\Delta_r| > \Delta_r^{\text{cr}}$  ( $|\Delta_r| < \Delta_r^{\text{cr}}$ ), the system is in an insulating (metallic) state. Note that for  $t' < 0.5t$  the system is in the insulating phase for any finite value of  $|\Delta_r|$ .

We complete our analysis by evaluating the ground-state charge distribution in the insulating phase. The average on-site charge density is

$$\langle n_i \rangle = 1 - (-1)^i \delta \rho_0, \quad (\text{A18})$$

where

$$\begin{aligned}\delta\rho_0 &= \frac{1}{L} \sum_{i,\sigma} [\langle n_{m,\sigma}^{(a)} \rangle - \langle n_{m,\sigma}^{(b)} \rangle] \\ &= \frac{1}{L} \sum_{k,\sigma} \cos 2\varphi_k [\langle \alpha_{k,\sigma}^\dagger \alpha_{k,\sigma} \rangle - \langle \beta_{k,\sigma}^\dagger \beta_{k,\sigma} \rangle] \quad (\text{A19})\end{aligned}$$

is the charge imbalance between “a” (odd) and “b” (even) sublattices (that is, the amplitude of the CDW pattern), induced by the ionic  $\Delta_r$  term.

In the band insulating ground state  $\langle \alpha_{k,\sigma}^\dagger \alpha_{k,\sigma} \rangle = 1$  and  $\langle \beta_{k,\sigma}^\dagger \beta_{k,\sigma} \rangle = 0$  for  $-\pi < k \leq \pi$ . Therefore,

$$\delta\rho_0 = \frac{1}{2\pi} \int_0^\pi dk \cos 2\varphi_k = \frac{\Delta_r \kappa K(\kappa)}{2\pi t}, \quad (\text{A20})$$

where  $K(\kappa)$  is the complete elliptic integral of the first kind with the modulus

$$\kappa = [1 + (\Delta_r/4t)^2]^{-\frac{1}{2}}. \quad (\text{A21})$$

## APPENDIX B: THE BAND INSULATOR PHASE

To assess the accuracy of the 2-FP approach, let us apply the bosonization analysis in the exactly solvable case of the free  $t$ - $t'$  ionic chain, where the Hubbard repulsion is included only via the renormalization of the ionic term. At  $U = 0$  the system is decoupled into the identical up and down spin component parts  $\mathcal{H} = \int dx [h_\uparrow + h_\downarrow]$ , where for each spin component the Hamiltonian is the sine-Gordon model with topological term

$$\begin{aligned}h_\sigma &= \frac{v_F}{2} [(\partial_x \phi_\sigma)^2 + (\partial_x \theta_\sigma)^2] - \frac{\mu_{\text{eff}}}{\sqrt{\pi}} \partial_x \phi_\sigma \\ &\quad - \frac{\Delta_r}{2\pi\alpha_0} \sin \sqrt{4\pi} \phi_\sigma, \quad (\sigma = \uparrow, \downarrow), \quad (\text{B1})\end{aligned}$$

with  $\mu_{\text{eff}}$  given by Eq. (13) in the main text. Each of these Hamiltonians is the standard one for the commensurate-incommensurate transition [36,37]. At  $\mu_{\text{eff}} = 0$ , the model is described by the theory of two commuting sine-Gordon fields with  $\beta^2 = 4\pi$ . In this case the excitation spectrum is gapped and the excitation gap is given by the mass of the up (down) field soliton  $M_\uparrow = M_\downarrow = \Delta_r/2$ . In the ground state the  $\phi_\uparrow$  and  $\phi_\downarrow$  fields are pinned with vacuum expectation values  $\langle 0 | \phi_\sigma | 0 \rangle = \sqrt{\pi}(n + 1/4)$ , with integer  $n$  giving the LRO in-phase distribution of electron density in the ground state

$$\rho_c(x) \simeq (-1)^n \frac{1}{\pi\alpha_0} \sum_\sigma \sin[\sqrt{4\pi} \phi_\sigma(x)]. \quad (\text{B2})$$

Thus, at low  $t' < 0.5t$  ( $\mu_{\text{eff}} = 0$ ) the ground state of the system corresponds to a CDW-type band insulator with a single energy scale given by the ionic potential  $\Delta_r$ .

At  $t' > 0.5t$  ( $\mu_{\text{eff}} \neq 0$ ) it is necessary to consider the ground state of the sine-Gordon model in sectors with nonzero topological charge. Competition between the chemical potential term (i.e.,  $t' > 0.5t$ ) and the commensurability energy given by  $\Delta_r$  finally drives a continuous phase transition from a gapped (insulating) phase at  $\mu_{\text{eff}} < \mu_{\text{eff}}^c$  to a gapless (metallic) phase at  $\mu_{\text{eff}} > \mu_{\text{eff}}^c$ , where

$$\mu_{\text{eff}}^c = \Delta_r/2. \quad (\text{B3})$$

Using Eq. (13) we easily obtain that the critical value of the n.n.n. hopping amplitude  $t'$ , obtained in the 2-FP approach from the condition (B3), coincides with the exact value given in (A15).

As we observe, the insulator-metal transition at  $t' > t'_c$  is connected with a change of the topology of the Fermi surface and a corresponding redistribution of the electrons from the lower (−) band into the upper (+) band. At the transition point the derivative of the ground-state energy with respect to the chemical potential displays a singular behavior of the usual square-root type  $\partial E_0/\partial\mu \sim -(\mu - \mu_c)^{1/2}$  when the chemical potential is constant, or linear dependence  $\partial E_0/\partial\mu \sim -(\mu - \mu_c)$  in the case of fixed particle density [56].

- 
- [1] M. Lewenstein, A. Sanpera, and V. Ahufinger, *Ultracold Atoms in Optical Lattices: Simulating Quantum Many-Body Systems* (Oxford University Press, Oxford, 2012).
  - [2] T. Esslinger, Fermi–Hubbard physics with atoms in an optical lattice, *Annu. Rev. Condens. Matter Phys.* **1**, 129 (2010).
  - [3] L. Tarruell and L. Sanchez–Palencia, Quantum simulation of the Hubbard model with ultracold fermions in optical lattices, *C. R. Phys.* **19**, 365 (2018).
  - [4] C. Chin, R. Grimm, P. Julienne, and E. Tiesinga, Feshbach resonances in ultracold gases, *Rev. Mod. Phys.* **82**, 1225 (2010).
  - [5] A. O. Gogolin, A. A. Nersisyan, and A. M. Tsvelik, *Bosonization and Strongly Correlated Systems* (Cambridge University Press, Cambridge, 1998).
  - [6] T. Giamarchi, *Quantum Physics in One Dimension* (Clarendon Press, Oxford, 2004).
  - [7] C. Becker, P. Soltan-Panahi, J. Kronjäger, S. Dörscher, K. Bongs, and K. Sengstock, Ultracold quantum gases in triangular optical lattices, *New J. Phys.* **12**, 065025 (2010).
  - [8] V. T. Phong, Z. Addison, S. Ahn, H. Min, R. Agarwal, and E. J. Mele, Optically controlled orbitronics on a triangular lattice, *Phys. Rev. Lett.* **123**, 236403 (2019).
  - [9] G.-B. Jo, J. Guzman, C. K. Thomas, P. Hosur, A. Vishwanath, and D. M. Stamper-Kurn, Ultracold atoms in a tunable optical kagome lattice, *Phys. Rev. Lett.* **108**, 045305 (2012).
  - [10] L. Tarruell, D. Greif, T. Uehlinger, G. Jotzu, and T. Esslinger, Creating, moving and merging Dirac points with a Fermi gas in a tunable honeycomb lattice, *Nature (London)* **483**, 302 (2012).
  - [11] T. Uehlinger, G. Jotzu, M. Messer, D. Greif, W. Hofstetter, U. Bissbort, and T. Esslinger, Artificial graphene with tunable interactions, *Phys. Rev. Lett.* **111**, 185307 (2013).
  - [12] E. Anisimovas, M. Račiūnas, C. Sträter, A. Eckardt, I. B. Spielman, and G. Juzeliūnas, Semisynthetic zigzag optical lattice for ultracold bosons, *Phys. Rev. A* **94**, 063632 (2016).
  - [13] J. H. Kang, J. H. Han, and Y. Shin, Realization of a cross-linked chiral ladder with neutral fermions in a 1D optical lattice

- by orbital-momentum coupling, *Phys. Rev. Lett.* **121**, 150403 (2018).
- [14] J. H. Kang, J. H. Han, and Y. Shin, Creutz ladder in a resonantly shaken 1D optical lattice, *New J. Phys.* **22**, 013023 (2020).
- [15] M. Ölschläger, G. Wirth, and A. Hemmerich, Unconventional superfluid order in the  $F$  band of a bipartite optical square lattice, *Phys. Rev. Lett.* **106**, 015302 (2011).
- [16] G. Wirth, M. Ölschläger, and A. Hemmerich, Orbital superfluidity in the P-band of a bipartite optical square lattice, *Nat. Phys.* **7**, 147 (2011).
- [17] M. Messer, R. Desbuquois, T. Uehlinger, G. Jotzu, S. Huber, D. Greif, and T. Esslinger, Exploring competing density order in the ionic Hubbard model with ultracold fermions, *Phys. Rev. Lett.* **115**, 115303 (2015).
- [18] R. Jördens, N. Strohmaier, K. Günter, H. Moritz, and T. A. Esslinger, Mott insulator of fermionic atoms in an optical lattice, *Nature (London)* **455**, 204 (2008).
- [19] E. Bertok, F. Heidrich-Meisner, and A. A. Aligia, Splitting of topological charge pumping in an interacting two-component fermionic Rice-Mele Hubbard model, *Phys. Rev. B* **106**, 045141 (2022).
- [20] A.-S. Walter, Z. Zhu, M. Gächter, J. Minguzzi, S. Roschinski, K. Sandholzer, K. Viebahn, and T. Esslinger, Quantization and its breakdown in a Hubbard–Thouless pump, *Nat. Phys.* **19**, 1471 (2023).
- [21] G. E. Volovik, Topological Lifshitz transitions, *Low Temp. Phys.* **43**, 47 (2017).
- [22] J. Ruhman and E. Altman, Topological degeneracy and pairing in a one-dimensional gas of spinless fermions, *Phys. Rev. B* **96**, 085133 (2017).
- [23] L. Gotta, L. Mazza, P. Simon, and G. Roux, Two-fluid coexistence and phase separation in a one-dimensional model with pair hopping and density interactions, *Phys. Rev. B* **104**, 094521 (2021).
- [24] S. Aditya and D. Sen, Bosonization study of a generalized statistics model with four Fermi points, *Phys. Rev. B* **103**, 235162 (2021).
- [25] C.-H. Huang, M. Tezuka, and M. A. Cazalilla, Topological Lifshitz transitions, orbital currents, and interactions in low-dimensional Fermi gases in synthetic gauge fields, *New J. Phys.* **24**, 033043 (2022).
- [26] C.-M. Halati and T. Giamarchi, Bose-Hubbard triangular ladder in an artificial gauge field, *Phys. Rev. Res.* **5**, 013126 (2023).
- [27] B. Beradze and A. A. Nersesyan, Spectrum, Lifshitz transitions and orbital currents in frustrated fermionic ladder with a uniform flux, *Eur. Phys. J. B* **96**, 2 (2023).
- [28] E. Müller-Hartmann, Ferromagnetism in Hubbard models: Low density route, *J. Low Temp. Phys.* **99**, 349 (1995).
- [29] M. Fabrizio, Superconductivity from doping a spin-liquid insulator: A simple one-dimensional example, *Phys. Rev. B* **54**, 10054 (1996).
- [30] K. Kuroki, R. Arita, and H. Aoki, Numerical study of a superconductor-insulator transition in a half-filled Hubbard chain with distant transfers, *J. Phys. Soc. Jpn.* **66**, 3371 (1997).
- [31] S. Daul and R. M. Noack, Phase diagram of the half-filled Hubbard chain with next-nearest-neighbor hopping, *Phys. Rev. B* **61**, 1646 (2000).
- [32] C. Aebischer, D. Baeriswyl, and R. M. Noack, Dielectric catastrophe at the Mott transition, *Phys. Rev. Lett.* **86**, 468 (2001).
- [33] M. E. Torio, A. A. Aligia, and H. A. Ceccatto, Phase diagram of the  $t$ - $t'$ - $U$  chain at half filling, *Phys. Rev. B* **67**, 165102 (2003).
- [34] G. I. Japaridze, R. M. Noack, D. Baeriswyl, and L. Tincani, Phases and phase transitions in the half-filled  $t$ - $t'$  Hubbard chain, *Phys. Rev. B* **76**, 115118 (2007).
- [35] S. Nishimoto, K. Sano, and Y. Ohta, Phase diagram of the one-dimensional Hubbard model with next-nearest-neighbor hopping, *Phys. Rev. B* **77**, 085119 (2008).
- [36] G. I. Japaridze and A. A. Nersesyan, Magnetic-field phase transition in a one-dimensional system of electrons with attraction, *JETP. Lett.* **27**, 356 (1978).
- [37] V. L. Pokrovsky and A. L. Talapov, Ground state, spectrum, and phase diagram of two-dimensional incommensurate crystals, *Phys. Rev. Lett.* **42**, 65 (1979).
- [38] J. Hubbard and J. B. Torrance, Model of the neutral-ionic phase transformation, *Phys. Rev. Lett.* **47**, 1750 (1981).
- [39] N. Nagaosa and J. Takimoto, Theory of neutral-ionic transition in organic crystals. I. Monte Carlo simulation of modified Hubbard model, *J. Phys. Soc. Jpn.* **55**, 2735 (1986).
- [40] T. Egami, S. Ishihara, and M. Tachiki, Lattice effect of strong electron correlation: Implication for ferroelectricity and superconductivity, *Science* **261**, 1307 (1993).
- [41] M. Fabrizio, A. O. Gogolin, and A. A. Nersesyan, From band insulator to Mott insulator in one dimension, *Phys. Rev. Lett.* **83**, 2014 (1999).
- [42] M. E. Torio, A. A. Aligia, and H. A. Ceccatto, Phase diagram of the Hubbard chain with two atoms per cell *Phys. Rev. B* **64**, 121105(R) (2001).
- [43] A. P. Kampf, M. Sekania, G. I. Japaridze, and P. Brune, Nature of the insulating phases in the half-filled ionic Hubbard model, *J. Phys.: Condens. Matter* **15**, 5895 (2003).
- [44] M. Tsuchiizu and A. Furusaki, Ground-state phase diagram of the one-dimensional half-filled extended Hubbard model, *Phys. Rev. B* **69**, 035103 (2004).
- [45] S. R. Manmana, V. Meden, R. M. Noack, and K. Schönhammer, Quantum critical behavior of the one-dimensional ionic Hubbard model, *Phys. Rev. B* **70**, 155115 (2004).
- [46] L. Tincani, R. M. Noack, and D. Baeriswyl, Critical properties of the band-insulator-to-Mott-insulator transition in the strong-coupling limit of the ionic Hubbard model, *Phys. Rev. B* **79**, 165109 (2009).
- [47] M. Sekania, S. Garuchava, J. Berakdar, and G. I. Japaridze, Mean-field ground-state phase diagram of the  $t$ - $t'$  ionic-Hubbard chain, [arXiv:2211.10543](https://arxiv.org/abs/2211.10543).
- [48] G. I. Japaridze, R. Hayn, P. Lombardo, and E. Müller-Hartmann, Band-insulator-metal-Mott-insulator transition in the half-filled  $t$ - $t'$  ionic Hubbard chain, *Phys. Rev. B* **75**, 245122 (2007).
- [49] G. I. Japaridze and A. A. Nersesyan, One-dimensional electron system with attraction in magnetic field, *J. Low Temp. Phys.* **37**, 95 (1979).
- [50] G. I. Japaridze, A. A. Nersesyan, and P. B. Wiegmann, Exact results in two-dimensional U(1)-Thirring model, *Nucl. Phys. B* **230**, 511 (1984).
- [51] I. Grusha, M. Menteshashvili, and G. I. Japaridze, Effective Hamiltonian for a half-filled asymmetric ionic Hubbard chain with alternating on-site interaction, *Int. J. Mod. Phys. B* **30**, 1550260 (2016).

- [52] F. D. M. Haldane, Spontaneous dimerization in the  $S = 1/2$  Heisenberg antiferromagnetic chain with competing interactions, *Phys. Rev. B* **25**, 4925 (1982).
- [53] K. Okamoto and K. Nomura, Fluid-dimer critical point in  $S = 1/2$  antiferromagnetic Heisenberg chain with next nearest neighbor interactions, *Phys. Lett. A* **169**, 433 (1992).
- [54] S. R. White, Density matrix formulation for quantum renormalization groups, *Phys. Rev. Lett.* **69**, 2863 (1992).
- [55] M. Fishman, S. R. White, and E. Miles Stoudenmire, The ITensor software library for tensor network calculations, *SciPost Phys. Codebases* **4** (2022).
- [56] T. Vekua, Susceptibility at the edge points of magnetization plateau of one-dimensional electron and spin systems, *Phys. Rev. B* **80**, 104411 (2009).
- [57] A. Richaud, M. Ferraretto, and M. Capone, Interaction-resistant metals in multicomponent Fermi systems *Phys. Rev. B* **103**, 205132 (2021).